MCR-82-530

Final Report May 1982

Evaluation and Prediction of Long-Term Environmental Effects on Nonmetallic Materials

Prepared for:

National Aeronautics and
Space Administration
Marshall Space Flight Center
Huntsville, Alabama 35812

MARTIN MARIETTA

MCR-82-530

Final
Report

May 1982

EVALUATION AND PREDICTION OF LONG-TERM ENVIRONMENTAL EFFECTS ON NONMETALLIC MATERIALS

MARTIN MARIETTA CORPORATION
DENVER AEROSPACE
P.O. Box 179
Denver, Colorado 80201

FOREWORD

This is the final report for a program of Evaluation and Prediction of Long-Term Space Environmental Effects on Nonmetallic Materials conducted by Martin Marietta for the National Aeronautics and Space Administration, Marshall Space Flight Center, under contract NAS8-33578.

The program was conducted in the Mechanical Materials Engineering Section with John A. Shepic initailly serving as Program Manager and Robert F. Geisendorfer serving subsequently. Contributors to the program included Charles E. Forsyth, and Jack Lebeau, of Martin Marietta.

Dr. Harold Papazian conducted data analyses and prepared the final report under the direction of Mr. Mohan Misra.

Don Gregory and Charles Stocks of NASA-MSFC conducted the charged-particle irradiations of the samples tested in the program. Mr. Charles Peacock was the technical monitor and Dr. Ray Gause and Ms. Ann Whitaker served as technical advisors.

CONTENTS

Figure

Table

MATERIALS LIST

Material	Manufacturer
Ablefilm 501	Ablestik Labs
Adlock 851	Am. Reinforced Plastics
Choseal 1224	Chromerics Inc.
Choseal 1236	Chromerics Inc.
DC93-500	Dow Corning Corp
DC6-1106	Dow Corning Corp
Diall FS-80, Type GOI-30	Miro Plastics Inc.
EA 934	Hysol
EA 956	Hysol
EA 9414	Hysol
EC 2216	3M
Eccofoam FPH	Emerson and Cuming, Inc.
FM 96U	Am. Cyanamid Co
HT 424	Am. Cyanamid Co
HT 435	Am. Cyanamid Co
Kapton F, 011	E. I. duPont
Kapton F, 919	E. I. duPont
Kynar Tubing	Raychem Corp
Lexan	General Electric Co
Nylon	E. I. duPont
Polyethylene	
Polythermalese Wire	Belden
Polyurethane	
Printed Circuit Board-Type GF	Synthane-Taylor Corp
Solithane 113	Thiokol Chem Corp
Stycast 1090	Emerson and Cuming, Inc.
Therm-Amid Wire	Rea Magnet Wire Co
Vespel SP-1	E. I. duPont
GFE (Graphite/Epoxy)	NASA-MSFC

APPLICATIONS INDEX

I. INTRODUCTION

Although nonmetallic materials are generally recognized as being susceptible to changes caused by the environments associated with long-life spacecraft, data concerning the effects of irradiation and long-term thermal-vacuum exposure in the specific mechanical, electrical, and thermal properties of such materials are not readily available. Since the performance and life of any structure, system, or component directly depends on the integrity of the materials used in its contruction, the ability of these materials to withstand the operating environment is of utmost importance to meeting the service life requirements.

The degradation of any material or material system, even if slow at normal use temperatures, can lead to failure over a long time period. For example, in a polymer system used as a structural member, the accumulated changes may eventually lead to loss of integrity. Degradation products may condense on optical parts and lead to system failure, and toxicity problems may become important if humans are exposed to the environment.

Real-time tests of materials that may be used in a system can be clearly impractical in time and money. If short-time tests can be used to predict future chemical and mechanical behavior, these tests can considerably enhance mission success. If properly evaluated and understood, the mechanisms of chemical change can be related to changes in mechanical properties. This offers an opportunity to devise rational accelerated tests from which the eventual changes in mechanical properties can be predicted.

Accelerated methods of predicting long-term thermal-vacuum aging effects have not been used with high confidence because their validity has not been tested by comparison with long-term real-time test data. The acceptance of an accelerated test method would increase the acceptance of nonmetallic materials for long-life spacecraft applications. However, long-term data for a large variety of nonmetallic materials have not been available.

The present program was undertaken in an attempt to overcome such problems by experimentally evaluating changes in functional properties of a broad spectrum of nonmetallic materials as a function of environment and exposure time, and to use such data in an attempt to develop models for predicting long-term material performance. Ancillary to this effort a literature search on specific materials, chosen by MSFC personnel, in the space and simulated space environment was carried and evaluated in a manner useful to designers in their selection of materials. The results of this survey are included as Appendix B.

The thermal-vacuum exposure part of the present experimental program has as its foundation the Viking materials qualification program of some nine years ago. The Viking project established the requirements for an extensive materials qualification test program and a unique thermal-vacuum exposure and test facility.

Approximately 300 nonmetallic materials were selected as candidates for the Viking project. These materials were then reviewed as to their intended applications, and critical mechanical, electrical, and thermal properties were selected for each material. Baseline values of each property were determined and additional samples of each material were then subjected to thermal-vacuum exposures ranging from one to 14 months. At intervals of one or three months, the same property determinations were made in situ to determine the influence of the earth-Mars cruise period on the performance of each material. At the conclusion of the program many samples of a wide variety of materials remained in the thermal-vacuum exposure cycle. A decision was then made to continue the thermal-vacuum exposures of these materials and to reestablish a test program to check the effects of long-duration exposures on the properties of these materials at some later date. Over 200 specimens of 40 different materials and some graphite/epoxy laminates provided by MSFC constituted the materials investigation of the present program.

II. EXPERIMENTAL TEST PROGRAM

A. THERMAL-VACUUM EXPOSURE AND TEST FACILITIES

The long-term vacuum exposures were accomplished in individual canisters connected to ion pumps. Four canisters are coupled directly to 50 ℓ/s ion pumps and the remaining 28 are connected to seven-canister plenums, with each plenum attached to a 400 ℓ/s ion pump. Each system is capable of maintaining pressures in the 10^{-7} to 10^{-8} torr range. Each canister is constructed of 300-series stainless steel, with a double wall for circulating water and maintaining the required thermal conditions in the canisters. A Marman clamp seals the lid to simplify remote opening and closing of the canisters in the test chamber. Two vacuum valves between the canister and vacuum plenum permit the canister to be removed from the pumping system and transferred to the test chamber without altering the pressure in the canister or plenum. A recirculating hot water heater maintains canister temperatures between ambient and +150°F. Figure 1 shows a typical seven-canister system.

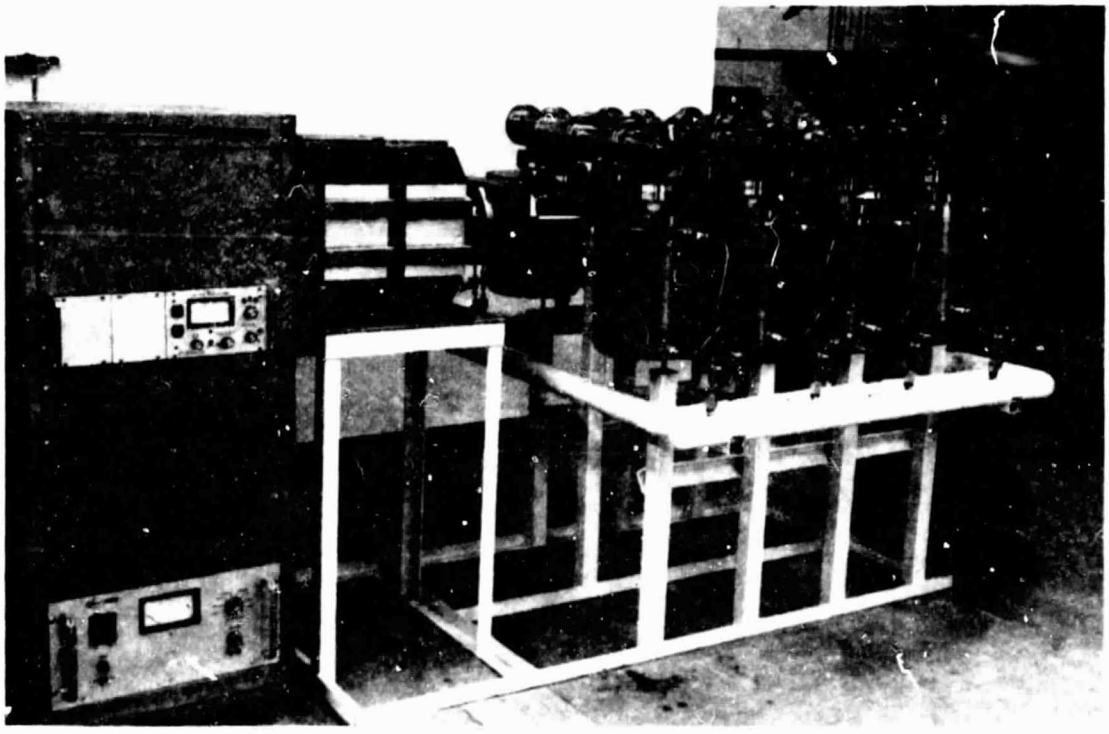

Figure 1 Seven-Canister Thermal-Vacuum Exposure System

The Vacuum *in situ* Test Chamber is constructed of 300 series stainless steel and consists of two individual vacuum chambers separated by a sliding gate valve. The main chamber is a nominal 5 feet in diameter and 7 feet long. The pumping portion of the main chamber consists of two 20-inch diffusion pumps with a multicoolant baffle and a valve isolating the pump from the chamber. The airlock pumping system consists of a 6-inch diffusion pump with a multicoolant baffle and isolation valve. The 6-square-foot chamber window has three tempered glass sections. A door on one end provides easy access to the entire chamber interior.

The unique feature of this system is the master/slave manipulation capability in the main chamber. Figure 2 shows three manipulators that enable access to over 90 percent of the chamber while it is evacuated. The manipulators are similar to those used in nuclear installations. The manipulators provide six degrees-of-freedom and have electric indexing in two axes for displacement of the master arm relative to the slave arm. All other motions are mechanical, with a one-to-one force ratio between the master arm and the slave arm except for the friction of the motion rods within the seal tube assembly.

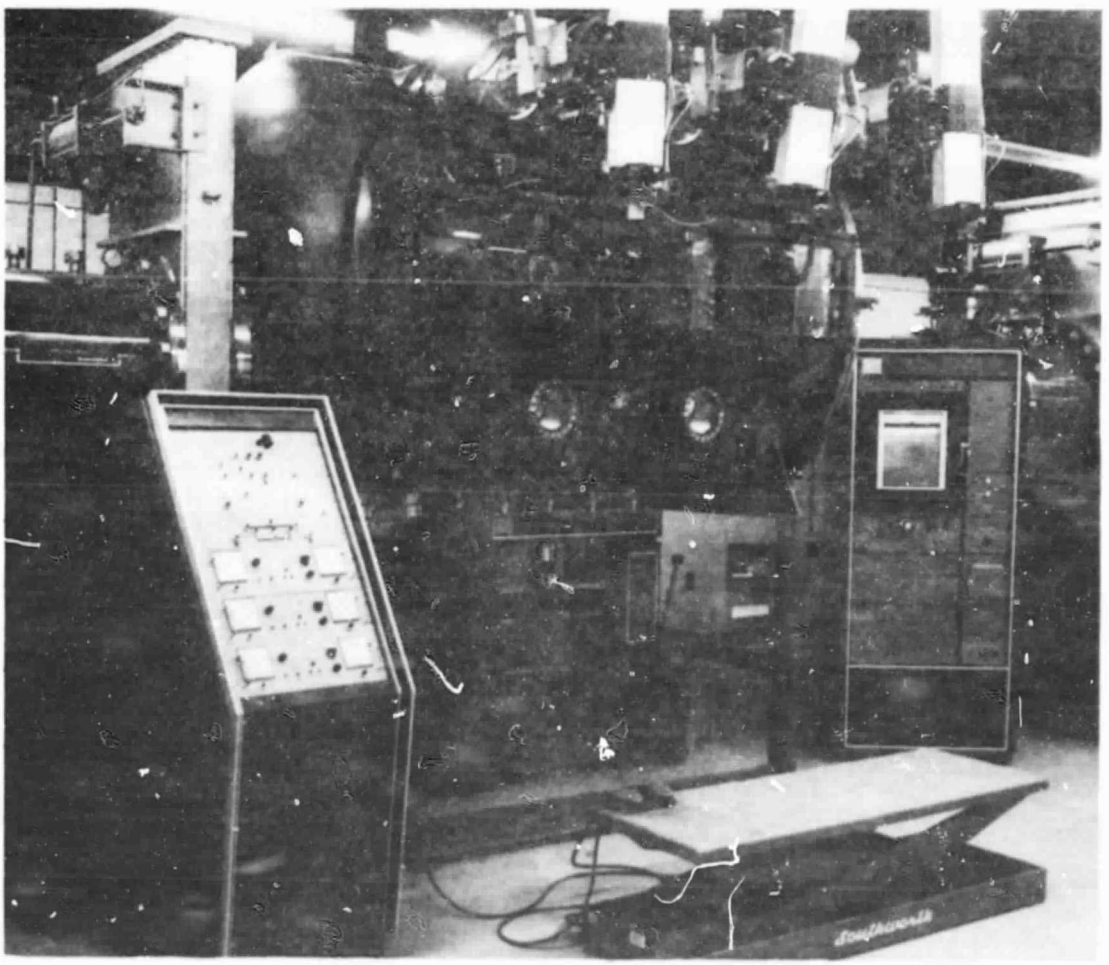

Figure 2 Vacuum in situ Test Chamber

Figure 3 shows an interior view of the chamber and the opening of a canister using the manipulator system.

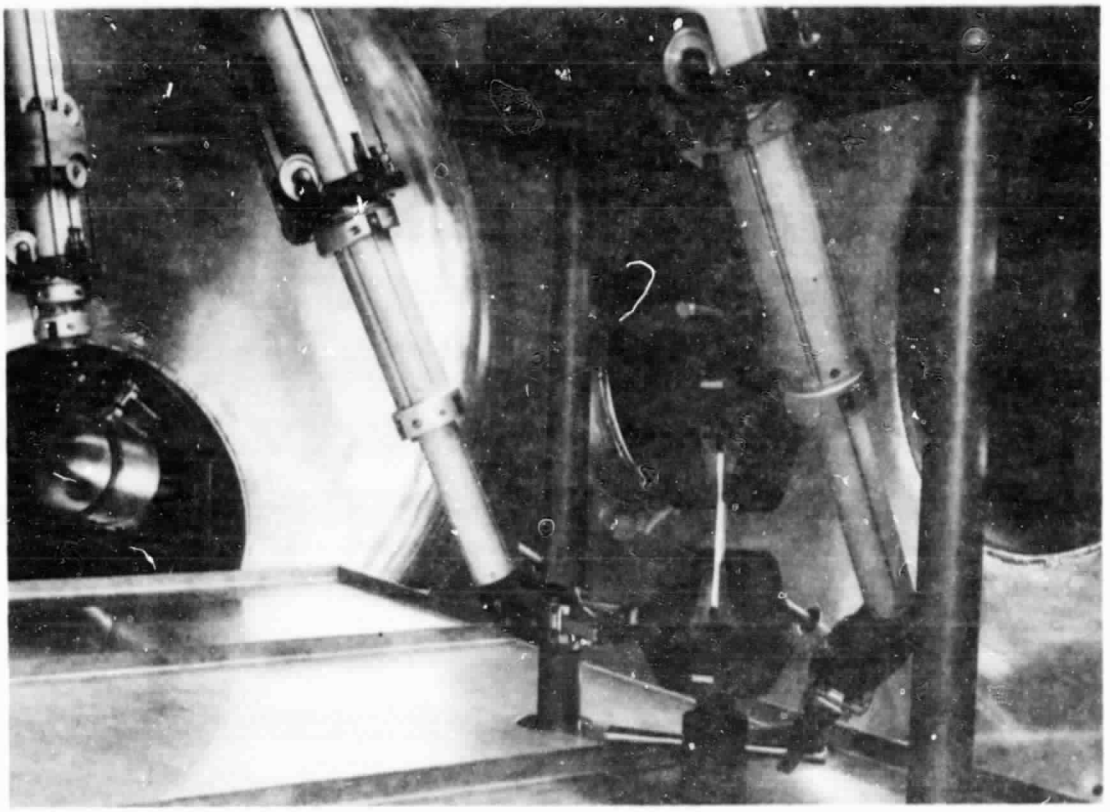

Figure 3 Interior of Chamber Showing Manipulators Preparing Tensile Test

A 10,000-lb Universal test machine is coupled to the main chamber. The columns are shock-isolated from the chamber with bellows and a moving crosshead pull rod is attached to the bellows. Tensile, compression, flexure, and shear tests have been performed in this chamber. Electrical property tests, including dielectric strength, dielectric constant, and surface and volume resistivity, have been conducted with the aid of special fixturing developed for use in vacuum with the master/slave manipulators.

After testing thermal-vacuum aged materials, samples were loaded under vacuum into a modified canister for transport to MSFC for electron irradiation. The modification allowed the canister to be evacuated continuously with a mobile ion pump system during transport between Denver and Huntsville and there to be directly coupled to the electron beam source. During transport the canister was maintained near 3×10^{-7} torr. After irradiation, the samples were returned in the same manner to Denver for testing. At this time the cycle was repeated with another canister loaded with other samples.

B. IRRADIATION FACILITIES

Marshall Space Flight Center personnel carried out the irradiations on their Van de Graff accelerator. After the canister was attached to the accelerator, which was maintained under a vacuum of about 3×10^{-6} torr, the valve on the canister was opened and the Van de Graff started. Because the beam was about 0.5 centimeters in diameter, it was scattered with two sheets of 0.001-inch Aluminum foil. This provided a beam of uniform intensity over a 6-inch diameter.

The current hitting the sample was measured using a Faraday cup designed by MSFC personnel. The current was kept generally in the manoamp range to minimize heating of the sample. By knowing the beam current and the exposure time, the fluence or the total number of electrons per square centimeter can be calculated.

After irradiation the canister with the specimens to be tested was replaced on the mobile ion pump system for transport from Huntsville to Denver.

III. TEST RESULTS

Over 200 specimens of 40 different materials that had been under thermal-vacuum exposure [150°F (338°k) at 10^{-6} torr] for some eight years were subjected to a variety of tests. The particular test (or tests) of a material was determined by the baseline tests obtained under the Viking materials program, i.e., if tensile data were available from the Viking program then the specimens were so tested in the present program, etc. All tests were conducted according to the appropriate ASTM method (see Appendix A, Table A-3, page A-2) except for thermal decomposition. The latter was tested via thermogravimetric analysis (TGA).

The TGA method is an accelerated test for characterization of thermal decomposition. This method involves taking a small amount of material through total decomposition by increasing the temperature on the sample at a predetermined rate (e.g., 10°C/min). Rate constants and activation energies for the decomposition can be determined from the data obtained. It has been demonstrated that such TGA results can be extrapolated to much lower temperatures to obtain thermal degradation near normal-use temperatures of samples of realistic size and weight. Isothermal (real-time) degradation kinetics on large samples near normal-use temperatures have been compared with results from TGA measurements. Remarkably accurate predictions can be made by TGA for degradations in vacuum (Ref 1) and in air (Ref 2).

Figure 4 shows a schematic multistage (here two-stage) TGA curve. It is appropriate to discuss here the construction of Table A-12 "Thermal Decompositions." In Table A-12 the number 2 in the column headed "Stages in the TGA Curve" refer to curves similar to that depicted in Figure 4. The number 1 indicates that only a one-stage degradation takes place through total decomposition, and the number 3 indicates an even more complex degradation than depicted in Figure 4, that is, a three-stage degradation through total decomposition. With multistage decompositions only the lowest temperature degradations (i.e., stage 1) were analyzed since this would be the one expected to dominate the near normal-use temperature isothermal decompositions. In the column labled "Reaction Mechanism in Stage 1", the a_o is the so-called "active component" in chemical kinetics terminology, and B represents the chemical component resulting from the degradation of a_o. Some materials show a simple mechanism, $a_o \rightarrow B$, of degradation while others show a complex mechanism, $a_o \rightarrow \begin{matrix} B \\ C \end{matrix}$ where a_o decomposes to B at the lower temperatures and $a_o \rightarrow C$ as the temperature increases within stage 1. Thus materials labeled 1 (i.e., single stage) a_o decomposes to B at the lower temperatures and $a_o \rightarrow C$ as the temperature increases within stage 1. Thus materials labeled 1 (i.e., single stage) and $a_o \rightarrow B$ have a simple reaction mechanism through total degradation. Materials labeled as multistage (i.e., 2 or 3) and $a_o \rightarrow \begin{matrix} B \\ C \end{matrix}$ will have an exceedingly complex degradation since the decomposition stage (or stages) at higher temperatures, which were not analyzed for the present study, may also degrade by complex routes such as $(d_o) \rightarrow \begin{matrix} E \\ F \end{matrix}$. The other columns are self-explanatory.

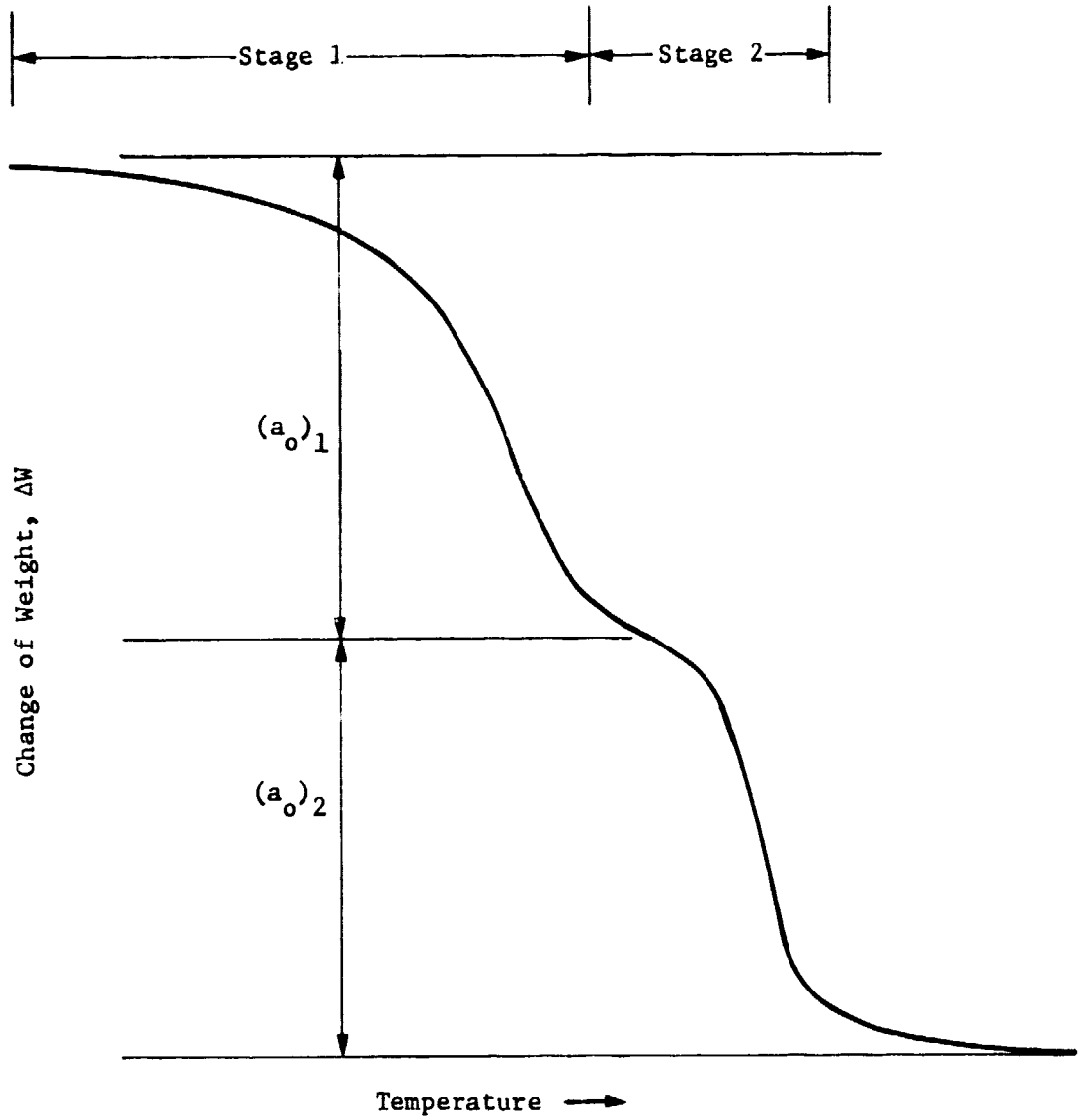

Figure 4 Schematic TGA Curve with a Two-Stage Decomposition

The test matrix is given in Table 1. It includes tests of the MSFC-supplied graphite/epoxy laminates. In Table 1 an x indicates baseline and thermal-vacuum data, and the o indicates data obtained after electron irradiations of specimens after long-term (>96 months) thermal-vacuum exposure. Comparison of this with the unirradiated long-term data gives some measure of the effect of electron irradiation.

Table 1 Materials Test Matrix

	Test (see Table 4, page A1)										
	1	2	3	4	5	6	7	8	9	10	11
Ablefilm 501		X									
EA 934		XO									X
EA 956		X									
EA 9414		X									
FM 96U		XO									
HT 424		XO									X
HT 435		XO									
EC 2216		X			XO						
Hysol C7-4248				X			X	XO	XO		
Stycast 1090								X			
Kapton F, 011	X										
Kapton F, 919	X										
Polythermalese Wire							X				
Therm-Amid Wire							X				
Vespel SP-1	X		X			XO	X	XO	XO	X	X
Choseal 1224										X	
DC 93-500								XO	O		
DC 6-1106					X						
Solithane 113		X									X
Eccofoam FPH								O	O		
Adlock 851	X		X								X
Diall FS-80								X	X		
Kynar Tubing							X				X
Print Circuit Board			X		X						
Lexan	XO										XO
Lucite	XO										XO
Polyurethane	XO										XO
Polyethylene	XO										X
Nylon	XO										XO
GFE Laminates											
010/049											X
005/063											X
009/055											X
004/044											X
Type 24				X							
Type 26				XO							
Type 37				X							
Type 38				XO							
Type 40				X							
Type 42				X							

X: Baseline and/or Thermal-Vacuum Exposure Tests.
O: Tests after Irradiation of Long-Term Thermal-Vacuum Specimens.

The data have been compiled (in Appendix A) in tables according to the tests performed. This allows easy comparision between materials and a particular property, e.g., tensile strength. Most of the data therein, for baseline and short-time (1-month/3-month) thermal-vacuum exposure, is from the Viking project of some eight years ago and is compiled in a Nonmetallic Materials Handbook (Ref 3). Not all of the results in the tables of Appendix A appear in Table 2, Summary of Results, because of a lack of appropriate data for comparison. This is especially true for the graphite/epoxy laminates where the data are only from the present study and could represent baseline data (i.e., unexposed to any environment) for some future study.

*Table 2 Summary of Results**

Materials \ Tests	Tensile		Lap Shear		Flexture		Compression		Peel		Hardness		Dielectric Strength		Dielectric Constant		Volume Resistivity		Activation Energy	
	S	L	S	L	S	L	S	L	S	L	S	L	S	L	S	L	S	L	S	L
Epoxy:																				
Ablefilm 501			+22	+8																
EA 934			+1	-5 (+2)																+4
EA 956				+2																
EA 9414				+16																
FM 96U			+4	-3 (+2)																
HT 424			+16	+8 (-8)																+39
HT 435			-7	-20 (-12)																
EC 2216			+1	+17						-48 (-50)										
Hysol C7-4248							-40	-47					-17	-12		(+5)				
Stycast 1090															-5	+9				
Polyimide:																				
Kapton F, 011		-9																		
Kapton F, 919		-5																		
Polytherm Wire																				
AWG 20													-8	+50						
AWG 30													-23	-1						
Therm-Amid Wire																				
AWG 20													-41	-11						
AWG 30													-19	+35						
Vespel SP-1	0	+12			+3	-10					-1	+1 (-1)	-30	-40	-2	-12 (+3)	35			+25
Silicone																				
Choseal 1224																	12	+45		
DC 93-500															-1	-3 (-22)				
DC 6-1106									-45	-50										
Polyurethane:																				
Solithane 113			-17	+10																+13
Eccofoam FPH																(-4)				
Phenolic:																				
Adlock 851		+25			+47	+73														+14
Graphite/Epoxy Laminate																				
Type 38							(16)**													
Type 26							(+57)**													
Miscellaneous:																				
Diall FS-80															10	-6				
Printed Circuit Board					+15	+18			-17	9										
Kynar Tubing													-49	-65						
	***																			
Lexan	-9	-12 (+7)																		-8 (+23)
Lucite	-12	-13 (-16)																		-2 (-2)
Polyurethane		-1 (-14)																		+42)
Nylon	+2	+30 (+12)																		(-29)
Polyethylene	0	-28 (+46)																		

* See text Results Section for details.
** See text.
*** Below this, List S is average of 3-month and 6-month exposures.

The values listed in Table 2 are the percent changes of the average values from the baseline average values taken from the data tables in the appendix. The column S is for short-time (1 or 3-month) thermal-vacuum exposure changes, and column L is for the approximately 8-year exposure changes. The values in parentheses are changes from the long-term property value after irradiation with electrons. The table is to be read in the following manner. For the first entry, Ablefilm 501, the lap shear strength increased by 22 percent after the short-time thermal-vacuum exposure. Over the years it decreased from the 22 percent to only 8 percent increase in lap shear strength over the baseline value. The bold print, **+22**, indicates no overlap in the spread of values from the five specimens tested and the spread of values from the baseline data and represents a real change. The normal print, +8, indicates an overlap of the spreads and may be taken to represent no change from the baseline value. For the seventh entry, HT435, the lap shear strength shows a decrease in lap shear strength of 20 percent over the years. The value in parentheses indicates that after electron irradiation the lap shear strength increased by 12 percent from the long-term exposure value so that after irradiation the lap shear strength was only 8 percent less than the average baseline value.

Some of the results in Table 2 are rather disconcerting. It would be expected that the primary result of thermal-vacuum exposure is the degassing of small fragment "solvents" such as monomer, catalyst, plasticizer, etc. This would then be expected to improve electrical properties and degrade a mechanical property, e.g., a flexure strength reduction. Yet in most of the materials the dielectric constants and lap shears have improved but the latter show changes somewhat larger than might be expected. Thus it appears more than simple degassing has taken place, and the relatively small thermal exposure [150°F (338 K)] causes changes in material properties over relatively short times (e.g., note the S column in lap shear strength and flexure). The electrical data (conductivity and dielectric constant) shown in Tables B-6 and B-7 of Appendix B are similar to the (disconcerting) results of the present study.

The results from the irradiation studies reported here must be used with caution since very few specimens were tested. However it is of interest to note that two very stable expoxies under thermal-vacuum exposure (EA934 and FM96U) show very little effect under irradiation. The graphite/epoxy laminate compression strength data must be considered only as a possible trend in results since for Type 38 only two irradiated specimens were available and for Type 26 only one specimen was available for the baseline data.

In view of the above discussion it is not possible to generate predictive models, but the value of the present study is twofold. It shows that real-time tests of materials must be planned with meticulous care as to sample preparation for a particular property, with exceedingly good record keeping to minimize experimental errors and test operator characteristics at some much later date. Secondly, and more importantly, it shows the value of developing meaningful accelerated tests such as those developed for thermal degradation (Ref 1 and 2) and for creep (Ref 4) to minimize the concerns outlined for real-time tests.

REFERENCES

1. H. A. Papazian: "Prediction of Polymer Degradation Kinetics at Moderate Temperatures from TGA Measurements." J. Appl. Polym. Sci. 16, 2503, 1972.

2. H. A. Papazian: "Predictive Testing of Nonmetallic Materials." SERI Contract XH-9-8191-1, 1980.

3. Nonmetallic Materials Handbook. NASA Contract NAS1-13177, Martin Marietta, Denver Aerospace, 1974.

4. H. A. Papazian: "Time Dependence of Polymer Strain in Air and in Vacuum." J. Appl. Polym. Sci., 18, 2311, 1974.

APPENDIX A

Table A-1 Test Methods

Test	ASTM
1. Tensile Strength	D638, D882
2. Lap Shear Strength	D1002
3. Flexure Strength	D790, C393
4. Compression Strength	D695, D3410
5. 180-deg Peel Strength	D1967, D903
6. Hardness	D785
7. Dielectric Strength	D149
8. Dielectric Constant	D150
9. Dissipation Factor	D150
10. Volume Resistivity	D257
11. Thermal Degradation	See Text

Table A-2 Notes for the Various Data Tables (As Labeled Therein)

Units:

ksi = psi x 10^{-3}
6.89 ksi = MPa (Mega-Pascals)
175 lb/in. = N/m (Newtons/meter)

Heat Compatibility (in N_2 Atmosphere):

(H) 570 h at 275°F (408 K)
(Ha) 380 h at 275°F (408 K)

Thermal-Vacuum Exposure after Heat Compatibility (H, or Ha), Specified Time (e.g., 1 mo/3 mo) at 150°F (338 K) and 10^{-6} torr:

(T) After (H) and Tested **in situ** (i.e., Vacuum)
(Ta) After (Ha) and Tested **in situ** (i.e., Vacuum)
(Tb) After (H) but Tested in Air
(Tc) After (H) Then Thermal-Vacuum Exposure in 10^{-6} torr but at 25°C (298 K), Tested **in situ** (i.e., Vacuum)

Irradiations with Electrons after Long-Term Exposure:

(R)	1 MeV	10^{14} electrons/cm^2
(R1)	1.5 MeV	10^{15} electrons/cm^2
(R2)	2.0 MeV	10^{15} electrons/cm^2
(R3)	2.5 MeV	10^{13} to 10^{15} electrons/cm^2

Table A-3 Tensile Strength

Material	Baseline	Heat Compat (H)*	1 mo/3 mo (T)*	Long-Term (T)*	After Irrad (R)*
Adlock 851 Ultimate Strength ksi	26.7 +1.2 −1.1	30.1 +5.3 −4.9		34 +4.7 −6.6	
MPa	184 +80 −70	208 +36 −34		234 +33 −45	
(Specimens) Date Tested	(5) 06/71	(5) 07/71		(5) 07/80	
Vespel SP-1	18 +0.7 −1.0	18.8 +1.0 −1.2	18.0 +1.2 −1.6	20.2 +1.3 −0.3	20.2 +0.3 −4.5
	124 +5.0 −7.0	129 +7.0 −8.0	124 +8.0 −11.0	139 +2.0 −2.0	139 +2.0 −36
	(5) 10/71	(5) 10/71	(5) 11/71	(5) 01/80	(3) 05/81
Kapton F, 919				(Tb)*	
	15 +1.50 −2.30	14.4 +2.0 −1.0		15.8 +2.7 −5.3	
	103 +10.3 −15.8	99.3 +13.8 −6.9		109 +18.6 −36.5	
	(5) 11/71	(5) 11/71		(5) 05/80	
Kapton F, 011	13.4 +3.0 −3.2	11.6 +3.7 −3.4		12.2 +2.8 −3.8	
	93.4 +20.7 −22.1	80 +25.5 −23.4		84 +19.3 −26.2	
	(5) 11/71	(5) 11/71		(5) 05/80	
Lucite		3 month (Tb)*	6 month (Tb)*	(Tb)*	(R)*
	12.9 +0.2 −0.7	10 +0.9 −0.67	12.5 +0.45 −1.00	11.2 +0.3 −0.4	9.38
	88.9 +1.4 −4.9	68.9 +6.1 −4.6	86.1 +2.2 −6.9	77.1 +1.2 −2.9	64.6
	(5) 03/72	(3) 06/72	(4) 09/72	(4) 05/80	(1) 05/81
Lexan	9.67 +0.79 −0.59	8.62 +1.03 −0.77	9.06 +0.29 −0.18	8.5 +0.08 −0.05	9.10 +0.27 −0.41
	66.7 +5.3 −4.2	59.4 +7.1 −5.3	62.4 +2.3 −1.2	58.5 +0.6 −0.3	62.6 +2.0 −2.8
	(5) 03/72	(4) 06/72	(4) 09/72	(4) 05/80	(4) 05/81
Polyurethane	8.14 +0.35 −0.34	Maximum Head Travel No Failures		8.04 +0.57 −0.36	6.87 +0.23 −0.17
	56.1 +2.3 −2.4			55.3 +5.9 −2.3	47.4 +1.5 −0.8
	(5) 03/72			(4) 05/80	(3) 05/81

Table A-3 (concl)

Material	Baseline	heat Compat (H)*	1 mo/3 mo (T)*	Long-Term (T)*	After Irrad (R)*
Nylon	8.63 $^{+0.37}_{-0.17}$	9.44 $^{+0.12}_{-0.08}$	8.20 $^{+0.22}_{-0.26}$	11.2 $^{+0.1}_{-0.1}$	12.6 $^{+0.2}_{-0.1}$
	59.3 $^{+2.7}_{-0.9}$	65.0 $^{+0.9}_{-0.5}$	56.5 $^{+1.5}_{-1.9}$	77.2 $^{+1.4}_{-1.4}$	86.8 $^{+1.4}_{-0.6}$
	(5) 03/72	(4) 06/72	(4) 09/72	(3) 05/80	(4) 05/81
Polyethylene	2.10 $^{+0.24}_{-0.34}$	2.80 $^{+0.03}_{-0.02}$	1.42 $^{+0.02}_{-0.02}$	1.52 $^{+0.45}_{-0.26}$	2.23 $^{+0.03}_{-0.01}$
	14.5 $^{+1.6}_{-2.4}$	19.3 $^{+0.20}_{-0.10}$	9.78 $^{+0.05}_{-0.05}$	10.5 $^{+3.30}_{-1.80}$	15.4 $^{+0.20}_{-0.10}$
	(5) 03/72	(4) 06/72	(4) 09/72	(4) 05/80	(3) 02/82

* See Table A-2.

Table A-4 Lap Shear Strength[+]

Material	Baseline	Heat Compat (H)*	1 mo/3 mo (T)*	Long-Term (T)*	After Irrad
Ablefilm 501 ksi	3.64 +0.30 −0.40	4.31 +0.29 −0.36	4.44 +0.14 −0.19	3.93 +0.43 −0.05	
MPa	25.1 +2.07 −2.76	29.7 +1.93 −2.48	30.6 +0.96 −1.31	27.1 +3.04 −0.34	
(Specimens) Date Tested	(5) 08/72	(5) 08/72	(5) 11/72	(5) 03/80	
EC 2216	4.05 +0.05 −0.12	3.18 +0.06 −0.04	4.07 +0.45 −0.47	4.75 +0.18 −0.21	
	27.9 +0.34 −0.83	21.9 +0.04 −0.03	28.1 +3.1 −3.2	32.7 +1.24 −1.45	
	(5) 10/71	(5) 12/71	(5) 01/72	(5) 01/80	
EA 934	2.42 +0.19 −0.26	2.14 +0.25 −0.20	2.45 +0.21 −0.16	2.29 +0.08 −0.17	(R1)* 2.34 +0.10 −0.12
	16.7 +1.31 −1.79	14.7 +1.72 −1.38	16.9 +1.45 −1.10	15.8 +0.55 −1.17	16.1 +0.69 −0.83
	(10) 10/71	(10) 10/71	(5) 11/71	(5) 01/80	(5) 05/81
EA 956	2.11 +0.11 −0.06	2.11 +0.13 −0.28		2.16 +0.11 −0.35	
	14.5 +1.0 −0.4	14.5 +0.9 −1.0		14.9 +0.70 −0.30	
	(3) 08/72	(3) 08/72		(3) 05/80	
EA 9414	5.32 +0.33 −0.32	6.48 +0.42 −0.24		6.19 +0.16 −0.31	
	36.6 +2.3 −2.2	44.6 +2.9 −1.6		42.6 +1.1 −2.2	
	(3) 08/72	(3) 08/72		(3) 05/80	
FM 960	3.28 +0.12 −0.07	3.44 +0.16 −0.24	3.42 +0.20 −0.20	3.17 +0.35 −0.57	(R2)* 3.24 +0.10 −0.10
	22.6 +0.83 −0.47	23.7 +1.10 −1.65	23.5 +1.38 −1.38	21.8 +2.40 −3.90	22.3 +0.70 −0.70
	(5) 11/71	(5) 12/71	(5) 01/72	(5) 01/80	(3) 02/82

Table A-4 (concl)

Material	Baseline	Heat Compat (H)*	1 mo/3 mo (T)*	Long-Term (T)*	After Irrad
HT 424					(R2)*
	3.17 $^{+0.11}_{-0.12}$	3.18 $^{+0.06}_{-0.03}$	3.68 $^{+0.07}_{-0.08}$	3.44 $^{+0.16}_{-0.14}$	3.15 $^{+0.28}_{-0.51}$
	21.8 $^{+0.76}_{-0.83}$	21.9 $^{+0.41}_{-0.20}$	25.3 $^{+0.48}_{-0.55}$	23.7 $^{+1.10}_{-0.96}$	21.7 $^{+1.90}_{-3.5}$
	(5) 11/71	(5) 12/71	(5) 01/72	(5) 01/80	(3) 02/82
HT 435					(R2)*
	2.46 $^{+0.12}_{-0.07}$	2.30 $^{+0.05}_{-0.13}$	2.29 $^{+0.13}_{-0.12}$	1.96 $^{+0.10}_{-0.11}$	2.19 $^{+0.08}_{-0.15}$
	16.9 $^{+0.83}_{-0.48}$	15.8 $^{+0.34}_{-0.90}$	15.8 $^{+0.90}_{-0.83}$	13.5 $^{+0.69}_{-0.75}$	15.1 $^{+0.50}_{-1.0}$
	(5) 11/71	(5) 01/72	(5) 01/72	(5) 01/80	(3) 02/82
HT 435 with Adlock 851 Adherends					
	2.04 $^{+0.12}_{-0.10}$	2.16 $^{+0.08}_{-0.08}$	2.10 $^{+0.10}_{-0.10}$	1.90 $^{+0.16}_{-0.16}$	
	14.1 $^{+0.83}_{-0.69}$	14.9 $^{+0.55}_{-0.55}$	14.5 $^{+0.69}_{-0.69}$	13.1 $^{+1.10}_{-1.10}$	
	(5) 11/71	(5) 01/72	(5) 01/72	(5) 01/80	
Solithane 113			(Tc)*	(Tc)*	
	0.30 $^{+0.07}_{-0.07}$	0.27 $^{+0.07}_{-0.07}$	0.25 $^{+0.02}_{-0.02}$	0.33 $^{+0.22}_{-0.14}$	
	2.07 $^{+0.48}_{-0.48}$	1.86 $^{+0.48}_{-0.48}$	1.73 $^{+0.14}_{-0.14}$	2.28 $^{+0.15}_{-0.10}$	
	(5) 09/71	(5) 09/71	(4) 12/72	(5) 01/80	

* See Table A-2.

+ All with 0.063 in. (0.16-cm) aluminum adherends (except as noted)--easily penetrated by the electron energies.

Table A-5 Flexure Strength

Material	Baseline	Heat Compat (H)*	1 mo/3 mo (T)*	Long-Term (T)*	After Irrad
Vespel SP-1					
ksi	19.2 $^{+0.6}_{-0.6}$	19.7 $^{+1.1}_{-0.7}$		17.2 $^{+0.5}_{-0.6}$	
MPa	132 $^{+4.1}_{-4.1}$	136 $^{+7.6}_{-4.8}$		118 $^{+3.4}_{-4.1}$	
(Specimens) Date Tested	(5) 10/71	(5) 10/71		(5) 01/80	
PC Board Copper-Clad Laminate					
	56 $^{+3.2}_{-1.5}$	55.8 $^{+5.4}_{-3.5}$	64.6 $^{+1.3}_{-0.9}$	66.4 $^{+1.9}_{-1.6}$	
	386 $^{+22.0}_{-10.3}$	384 $^{+37.2}_{-24.1}$	445 $^{+9.0}_{-6.2}$	457 $^{+13.1}_{-11.0}$	
	(5) 02/72	(5) 02/72	(5) 03/72	(5) 06/80	
Adlock 851					
	59.1 $^{+1.5}_{-2.2}$	50.1 $^{+1.4}_{-1.5}$	87.4 $^{+3.0}_{-6.1}$	102 $^{+3.0}_{-2.2}$	
	407 $^{+9}_{-8}$	345 $^{+10}_{-10}$	600 $^{+23}_{-39}$	704 $^{+21}_{-16}$	
	(5) 10/71	(5) 10/71	(5) 11/71	(5) 04/80	

*See Table A-2.

Table A-6 Compression Strength

Material	Baseline	Heat Compat (H)*	1 mo/3 mo (T)*	Long-Term (T)*	After Irrad
Hysol C7-4248					
ksi	31.5 $^{+2.2}_{-2.3}$	28.5 $^{+4.1}_{-3.9}$	18.7 $^{+2.0}_{-6.1}$	16.7 $^{+5.9}_{-6.2}$	
MPa	217 $^{+15.2}_{-15.8}$	196 $^{+28.3}_{-26.9}$	129 $^{+13.8}_{-42.0}$	115 $^{+41}_{-43}$	
(Specimens) Date Tested	(4) 01/72	(5) 01/72	(5) 02/72	(5) 01/80	
Graphite/Epoxy Laminates					(See Text)
Type 38	56.6 $^{+3.0}_{-4.1}$				47.5 $^{+2.8}_{-2.8}$
	390 $^{+21}_{-34}$				327 $^{+19}_{-19}$
	(3) 03/82				(2) 02/82
Type 26	29.7				(See Text) 46.7 $^{+10}_{-7.7}$
	205				322 $^{+69}_{-54}$
	(1) 03/82				(10) 02/82
Type 24	33.9 $^{+3.6}_{-2.5}$				
	234 $^{+24}_{-18}$				
	(3) 03/82				
Type 37	44.2 $^{+10.5}_{-7.2}$				
	304 $^{+73}_{-59}$				
	(3) 03/82				
Type 40	37.9 $^{+10.1}_{-8.2}$				
	261 $^{+70}_{-56}$				
	(3) 03/82				
Type 42	47 $^{+7.3}_{-7.3}$				
	324 $^{+50}_{-50}$				
	(2) 03/82				

* See Table A-2.

Table A-7 180-Degree Peel Strength

Material	Baseline	Heat Compat (H)*	1 mo/3 mo (T)*	Long-Term (T)*	After Irrad (R)*
DC6-1106					
lb/in.	28 +16 −10	40 +2 −4	15.4 +2.1 −0.9	14 +1.5 −1.5	
N/m (10^{-3})	4.9 +2.8 −1.8	7.0 +0.35 −0.70	2.7 +0.37 −0.16	2.4 +0.26 −0.26	
(Specimens) Date Tested	(5) 09/71	(5) 09/71	(5) 10/71	(5) 05/80	
EC-2216					
	37 +7.0 −9.0			19 +7.0 −12.0	9.5 +2.5 −1.5
	6.47 +1.22 −1.58			3.33 +1.22 −2.10	1.66 +0.44 −0.26
	(10) 07/71			(5) 01/80	(3) 05/81
PC Board Copper Peel					
	1.85 +0.5 −0.3	1.57 +0.11 −0.07	1.53 +0.07 −0.03	1.69 +0.41 −0.19	
	0.32 +0.09 −0.05	0.27 +0.02 −0.01	0.27 +0.01 −0.05	0.30 +0.07 −0.03	
	(11) 02/72	(12) 02/72	(12) 03/72	(20) 06/80	

* See Table A-2.

Table A-8 Hardness

Material	Baseline	Heat Compat (H)*	1 mo/3 mo (T)*	Long-Term (T)*	After Irrad (3)*
Vespel SP-1					
Rockwell-M	88.2 +0.8 −1.2	90.0 +2.0 −1.0	89.6 +0.4 −2.6	87.2 +1.8 −2.2	
Shore-D	86 +0 −1.0	86 +0 −0	85 +1 −0	87 +1 −1	86 +1 −0
(Specimens) Date Tested	(5) 10/71	(5) 10/71	(5) 11/71	(4) 01/80	(3) 05/81

* See Table A-2.

Note:

Rockwell-M tester could not be used in situ - Rockwell tests carried out after Shore-D Test.

Table A-9 Dielectric Strength

Material	Baseline	Heat Compat (H)*	1 mo/3 mo (T)*	Long-Term (T)*	After Irrad
Vespel SP-1					
V/mil	676 +28 −22	666 +76 −44	469 +25 −111	405 +38 −18	
V/m (10^{-7})	2.7 +0.1 −0.1	2.6 +0.3 −0.2	1.9 +0.2 −0.4	1.6 +0.1 −0.1	
(Specimens) Date Tested	(5) 12/71	(5) 12/71	(5) 01/72	(5) 06/80	
Hysol C7-4248					
	2.32 +0.17 −0.44	2.33 +0.31 −0.31	1.93 +0.32 −0.23	2.03 +0.02 −0.03	
V/m (10^{-4})	9.1 +0.73 −1.70	9.2 +1.2 −1.2	7.6 +1.25 −0.90	8.0 +0.06 −0.12	
	(5) 05/72	(5) 05/72	(5) 06/72	(3) 03/80	
Knynar Tubing					
	1.37 +0.04 −0.02	1.37 +0.12 −0.15	0.7 +0.04 −0.05	0.48 +0.02 −0.03	
V/m (10^{-4})	5.4 +0.14 −0.07	5.4 +0.46 −0.60	2.78 +0.13 −0.22	1.89 +0.08 −0.12	
	(5) 05/72	(5) 05/72	(5) 07/72	(5) 03/80	
Polythermalese Wire					
AWG 20 KV	9.5 +1.7 −1.4	10.1 +1.4 −0.7	8.7 +3.0 −1.5	14.3 +2.2 −2.3	
AWG 30	8.8 +2.3 −1.8	7.6 +0.5 −0.4	6.8 +0.4 −0.3	8.7 +0.8 −0.7	
	(3) 05/72	(3) 05/72	(3) 06/72	(3) 07/80	
Therm-Amid Wire					
AWG 20 KV	12.7 +1.8 −1.7	8.5 +0.5 −0.5	7.5 +0 −0.1	11.3 +0.2 −0.3	
AWG 30	8.0 +1.5 −1.0	8.7 +1.1 −0.6	6.5 +0 −0.1	10.8 +0.7 −0.8	
	(3) 05/72	(3) 05/72	(3) 06/72	(3) 07/80	

* See Table A-2.

Table A-10 Dielectric Constant/Dissipation Factor

Material	Baseline	Heat Compat (H)*	1 mo/3 mo (T)*	Long-Term (T)*	After Irrad (R)*
Vespel SP-1					
Dielectric Const	2.94	2.91	2.87	2.44	2.52
Dissip Factor	0.00046	0.00109	0.00016	0.0013	0.0024
(Specimens) Date Tested	(3) 12/71	(3) 12/71	(3) 01/72	(3) 04/80	(3) 03/81
Ecco Foam FPH				1.14	1.095
				0.004	0.0077
				(3) 06/80	(3) 03/82
Hysol C7-4248			2.997	3.065	3.238
			---	0.0084	0.0047
			(3) 12/71	(2) 04/80	(1) 03/81
Diall FS-80		(Ha)*	(Ta)*	(Ta)*	
	3.79	3.60	3.43	3.49	
	0.012	0.009	0.002	0.004	
	(3) 06/72	(3) 06/72	(3) 07/72	(2) 04/80	
Stycast 1090	2.89	2.82	2.75	3.17	
	---	---	---	---	
	(3) 10/72	(3) 01/72	(3) 04/72	(3) 04/80	
DC 93-500	2.79	2.76	2.76	2.79	1.985
	---	---	---	0.0043	0.0026
	(2) 12/71	(4) 12/71	(4) 03/72	(3) 04/80	(1) 03/81

Table A-11 Volume Resistivity

Material	Baseline	Heat Compat (H)*	1 mo/3 mo (T)*	Long-Term (T)*	After Irrad
Choseal 1224 ohm-cm (Specimens) Date Tested	6.2 $^{+3.6}_{-3.2}$ (3) 12/71	5.9 $^{+2.1}_{-1.0}$ (3) 12/71	4.8 $^{+0.1}_{-0.3}$ (3) 01/72	9.0 $^{+4.7}_{-3.1}$ (3) 04/80	
Vespel SP 1 (10^{-14})	6.67 $^{+3.33}_{-1.67}$ (3) 12/71	2.83 $^{+2.17}_{-1.33}$ (3) 12/71	3.01 $^{+0.13}_{-0.27}$ (3) 01/72		
See Table A-2.					

Table A-12 Thermal Decomposition

Material	Stages in TGA Curve*	Reaction Mechanism* in Stage 1	Stage 1 Temp Range, °C	Activation Energy, kcal, (kJ)		
				Baseline	Long-Term	After Irrad
Solithane	3	$a_o \rightarrow B$	25-250	23 (96)	26 (109)	
EA934	2	$a_o \rightarrow B$	25-400	70 (293)	73 (305)	
HT424	1	$a_o \rightarrow B$, $a_o \rightarrow C$	25-500	11 (46)	18 (75)	
Vespel SP-1	1	$a_o \rightarrow B$, $a_o \rightarrow C$	450-650		86 (360)	108 (450)
Kapton F,919	2	$a_o \rightarrow B$	300-550		52 (218)	
Adlock 851	1	$a_o \rightarrow B$	250-650	14 (59)	16 (62)	
Kynar Tubing	2	$a_o \rightarrow B$	300-450		48(201)	
DC 93-500	3	$a_o \rightarrow B$	25-550			25 (105)
DC 6-1106	2	$a_o \rightarrow B$	25-550	25 (105)		
Choseal 1224	1	$a_o \rightarrow B$	330-720	24 (100)		
Lucite	1	$a_o \rightarrow B$	125-400	43 (180)	42 (176)	41 (171)
Nylon	1	$a_o \rightarrow B$	200-400		65 (272)	46 (192)
Lexan	1	$a_o \rightarrow B$	200-500	52 (218)	48 (201)	
	2	$a_o \rightarrow B$, $a_o \rightarrow C$	140-450			59 (247)
Polyurethane	2	$a_o \rightarrow B$	125-250		24 (100)	34 (142)
Polyethylene	3	$a_o \rightarrow B$	150-400		118 (490)	
GFE 010/049	1	$a_o \rightarrow B$, $a_o \rightarrow C$	25-450	23 (96)		
005/063	1	$a_o \rightarrow B$, $a_o \rightarrow C$	25-450	23 (96)		
009/055	1	$a_o \rightarrow B$, $a_o \rightarrow C$	25-450	18 (75)		
004/044	1	$a_o \rightarrow B$, $a_o \rightarrow C$	25-450	18 (75)		

* See text.

APPENDIX B

LITERATURE SEARCH

APPENDIX B - LITERATURE SEARCH

A computer-assisted literature search was carried out in the NASA and DOD data banks for space environmental effects on the three types of spacecraft materials specified by the COR. The materials chosen by the COR were Kapton, Teflon, and silicones, including the S-13 and S-13G paints. The information developed includes flight and laboratory test data. The search developed 132 references of which approximately 70 were surveyed for the three subject materials.

Significant quantities of information were obtained from three sources. A large amount of laboratory data on chemical and physical properties was developed by Martin Marietta Denver Aerospace during the Viking project and compiled into a handbook. Pertinent pages from this handbook are referenced in the appropriate sections. Boeing Aerospace conducted extensive irradiation studies of thermal control coatings during the 1965-1968 period. Much of their information on S-13 and S-13G will also be referred to later. An extensive report by TRW, Properties of Metalized Flexible Materials in the Space Environment, was published in 1978. It contains much information on Teflon and Kapton and will be referred to in the appropriate paragraphs. Other reports and compilations will also be discussed; however, references within compilations will not be referred to as they can be found in the particular compilation.

A. SILICONES AND THE S-13 AND S-13G THERMAL CONTROL PAINTS

1. Silicones

Because silicones do not contain the variety of secondary additives common to most organics, thermal-vacuum exposure does not significantly alter their physical and electrical properties. Dimethyl silicones display greater stability to ultraviolet degradation than the phenyl-containing silicones, which is the opposite behavior of particle radiation stability. The photon-irradiated phenyl-based materials show measurable surface effects of cracking, crazing, and discoloration. However, low-temperature (-90°C flexibility) properties are imparted to silicone elastomers by a small but optimum number of phenyl groups. The more bulky phenyl groups break up the regularity of the polymethylsiloxane chain necessary for crystallitic growth. Particle irradiation in high doses (10 to 100 megarads) causes increased hardness and tensile strength and appreciably reduces elongation of silicone elastomers. The higher phenyl-containing elastomers are more resistant to such effects. (Ref 1).

A recent compilation (Ref 2) of vacuum-condensible materials (VCM) data shows silicone rubbers to sustain a total weight loss (TWL) ranging between 0.1 to 3.5 percent and a VCM ranging from 0.00 to 0.8 percent when exposed to thermal-vacuum for 24 hours at 125°C under 10^{-6} torr vacuum.

The thermal decompositions in vacuum follow (Ref 3, 4) simple first-order kinetics with the rate equation given by

$$\frac{dx}{dt} = k_T (a_o - x)$$

where k_T is the rate constant at temperature T, dx/dt is the rate of weight loss, and a_o-x is the concentration and a_o is the initial concentration. It has been shown that the same rate equations hold for decompositions in air. (Ref 5).

The activation energies for thermal decomposition of silicones in vacuum do not exceed about 30 kcal. This can be ascertained from the pages from the Martin Marietta handbook (Ref 4) of Viking data referenced in the following tabulation.

Material	Pages (Inclusive)
Cho-Seal 1224	S-1 - S-9
DC6-1102	S-10 - S-13
DC6-1104	S-14 - S-17
DC6-1106	S-19 - S-22
DC92-007	S-23 - S-28
DC93-500	S-29 - S-33
MS40G08	S-34 - S-37
Silicone Tape, Series 600	S-38 - S-42
RTV-511, Modified	S-43 - S-48
ZP5044 Silicone Gasket	S-49 - S-52

As mentioned earlier, the effect of thermal-vacuum exposure on the physical properties of silicones is expected to be slight as shown by the Viking data referenced above. Concordant with these data are the results (Ref 1) for a test of Young's modulus in flexure stiffening temperature (stiffening temperature defined as the point where Young's modulus reaches 10,000 psi). A general-purpose silicone RTV and a clear rubbery-resinous silicone showed no change in the stiffening temperature after exposure for one week at 150°C under 10^{-7} torr vacuum.

Laboratory studies (Ref 6) of ultraviolet irradiation have shown that only the polydimethylsiloxanes (RTV-615 and O-I type 650) are resistant to degradation when exposed to solar radiation. After 800 ESH (equivalent solar hours) there was no significant degradation with $\Delta\alpha_s$ = 0.005 to 0.008. The SR series all degraded by 100 ESH with $\Delta\alpha_s$ = 0.044 to 0.061. A test sample of methyl silicone was flown (Ref 7) on OSO-III along with samples of thermal control coatings. Over approximately 2700 ESH, α_s changed by 0.11 but there was no apparent change up to about 200 ESH.

The decrease in transmittance over the wavelength range 0.4 to 2.5 of DC 92-009 under proton irradiation has been studied (Ref 8). For μ 150-keV protons at irradiation rates between 6.6×10^{10} and 6.6×10^{13} protons/cm^2/s, the transmittance is given by

$T = 11.78\ E^{-0.134}$

within ± 5 percent for total energy, E, deposited between 10^8 and 10^{10} ergs/cm^2. For 50-keV protons at rates of 6.6×10^{11} and 6.6×10^{12} protons/cm^2/s,

$T = 5.29\ E^{-0.0935}$

over the same total deposited energy.

2. S-13 and S-13G Thermal Control Paints

a. Ultraviolet Radiation - Through 1966 an experiment on OSO-II provided the most extensive data for thermal coatings on a near-earth satellite (Ref 9). At that time the changes in α_s were attributed to changes in the near-infrared reflectance. That this is indeed the case is shown in Figure B-1 taken from the extensive report of the Boeing group (Ref 10). The recovery shown in the figure occurs after backfilling the vacuum irradiation chamber with dry air. Some changes in α_s have been collected in Table B-1.

The large changes in α_s on the Skylab experiment have been attributed to a combination of contamination and solar degradation (Ref 11). The OSO-III results are in good agreement with OSO-II as well as Pegasus I results, but the changes in α_s are much less than for Mariner V and the difference is attributed (Ref 7) to solar wind effects on Mariner V.

The Boeing group has done extensive work (Ref 10) on electromagnetic and particle radiation on S-13 and S-13G-type coatings. For ultraviolet radiation they used mercury arc (four GE U-11 and two UA-3 lamps) and xenon long-arc sources. With S-13 the xenon source showed much more damage (changes in reflectance through the wavelength range 0.25 to 2.5 μ) for 85 ESH than 135 ESH of the mercury arc. Only between 0.4 and 0.5 μ is the buildup greater with the 135 ESH of the mercury source. Significant reflection losses occur in both S-13 and S-13G. Figures B-2 and B-3 show these changes (Ref 10). The S-13G, which undergoes smaller changes in the IR, exhibited little recovery even after seven days of backfilled air in the vacuum irradiation chamber. The S-13 had nearly complete recovery (Fig. B-1). In the visible region S-13G showed no recovery and S-13 only a slow partial recovery.

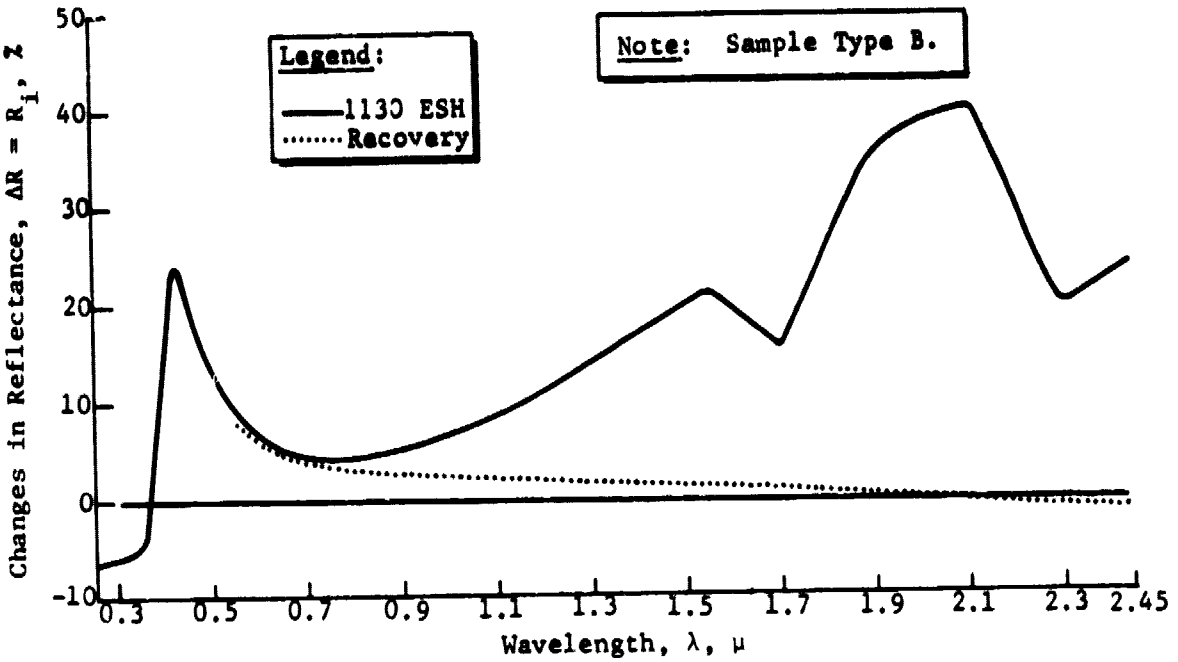

Figure B-1
Reflectance Recovery of S-13 in Air As a Function of Wavelength Following Exposure to Ultraviolet Radiation (Ref 10)

Table B-1 Changes in α_s Under Solar Radiation

S-13 Type			
Hours	$\Delta\alpha_s$	Flight	Ref
2000	0.12	OSO-II	9
2400	0.14	OSO-III	7
2040	0.284	Skylab D024	11
700	0.11	Lunar Orbiter II	12
800 ESH	0.8	Lab (IITRI)	12
1330	0.10	Lab (LMSC)	12
1098 at 18 Suns	0.61	Lab (IITRI)	12

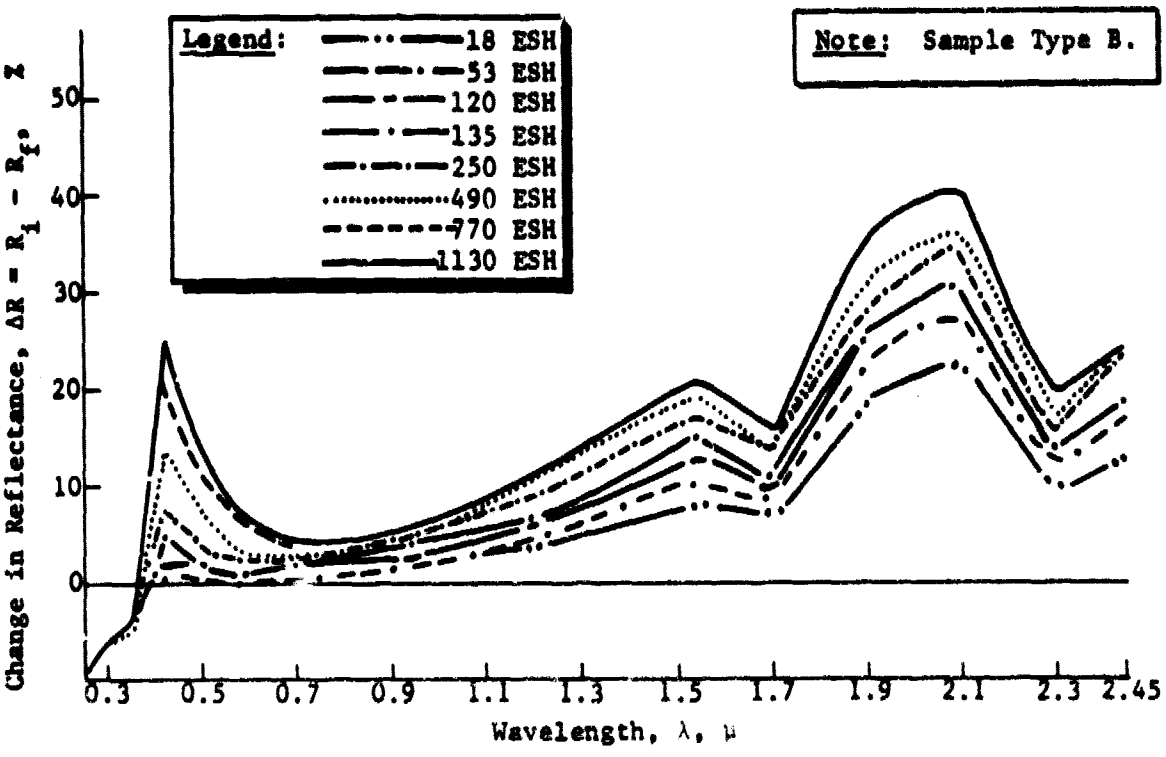

Figure B-2
Spectral Reflectance Changes in Zinc Oxide-Methyl Silicone, S-13, Following Exposure to Ultraviolet Radiation (Ref 10)

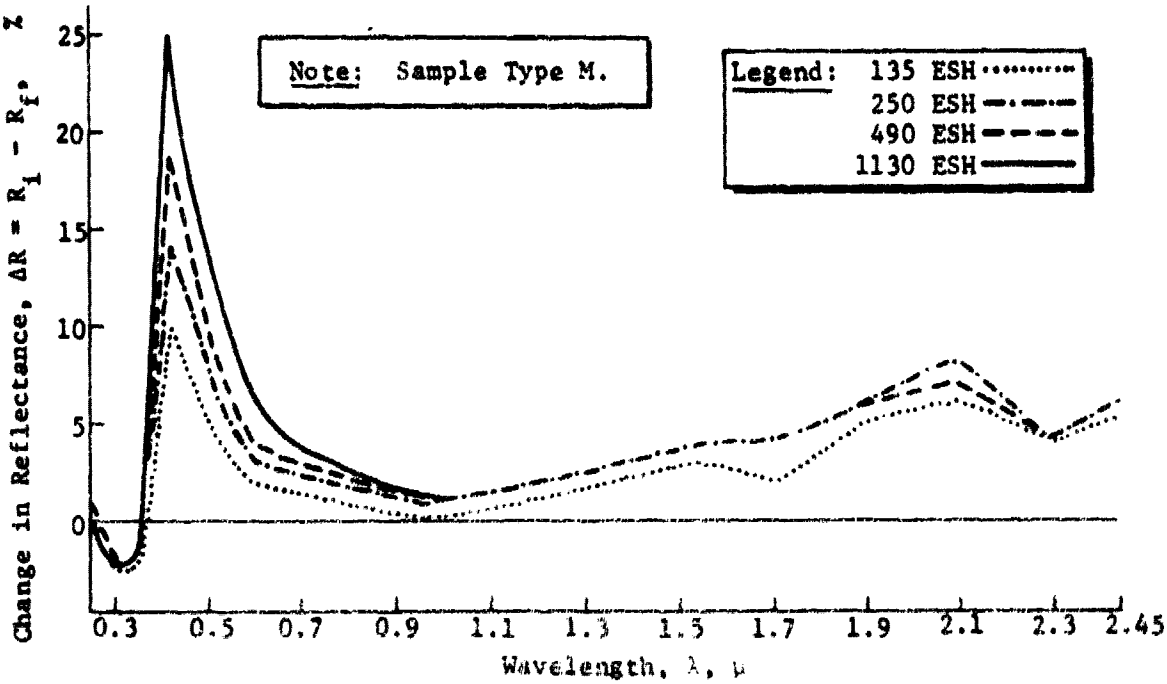

Figure B-3
Spectral Reflectance Changes in an Early Formulation of S-13G, Treated Zinc Oxide-Methyl Silicone, Following Exposure to Ultraviolet Radiation (Ref 10)

Degradation rate studies of the infrared reflection with S-13 showed (Ref 13) that the rate increases as the incident radiation decreases from 3500 to 2200 Å. With 2600 ± 200 Å radiation, the rate is proportional to $\sqrt{I + I}$. The effect of total dose is not constant but is affected independently by intensity and time.

Some other laboratory and flight data are presented in Table B-2 for S-13G-type coatings. For the Skylab results, the same contamination comment holds here as for the S-13 results in Table B-1.

Table B-2
Changes in α_s Under Solar Radiation

S-13G			
Hours	$\Delta\alpha_s$	Flight	Ref
2400	0.07	OSO III	5
2040	0.237	Skylab D024	8
900	0.14	Lunar Orbiter I	9
600	0.09	Lunar Orbiter II	9
1300 ESH	0.8	Lab	9
600	0.01	Lab	

b. Electron Irradiation - The Boeing group (Ref 10) found that over wide ranges of fluxes and fluences (4×10^8 to 1.7×10^{12} electrons/ cm^2/s and 10^{13} to 8×10^{15} electrons/cm^2), no irradiation rate effects from 50-keV electrons are evident from in situ measurements of hemispherical spectra reflectance obtained with an integrating sphere reflectometer. Thus to an acceleration factor of 10^3 or so, laboratory exposures of S-13 and S-13G coatings to 50-keV electrons at rates greater than those in space are valid.

After exposure to electron irradiation, S-13 and S-13G recover reflectance losses when exposed to dry air (Fig. B-4). However, when exposed to 8×10^{15} electrons/cm^2, "permanent" damage remains even days after exposure to air. Figure B-5 shows the early recovery.

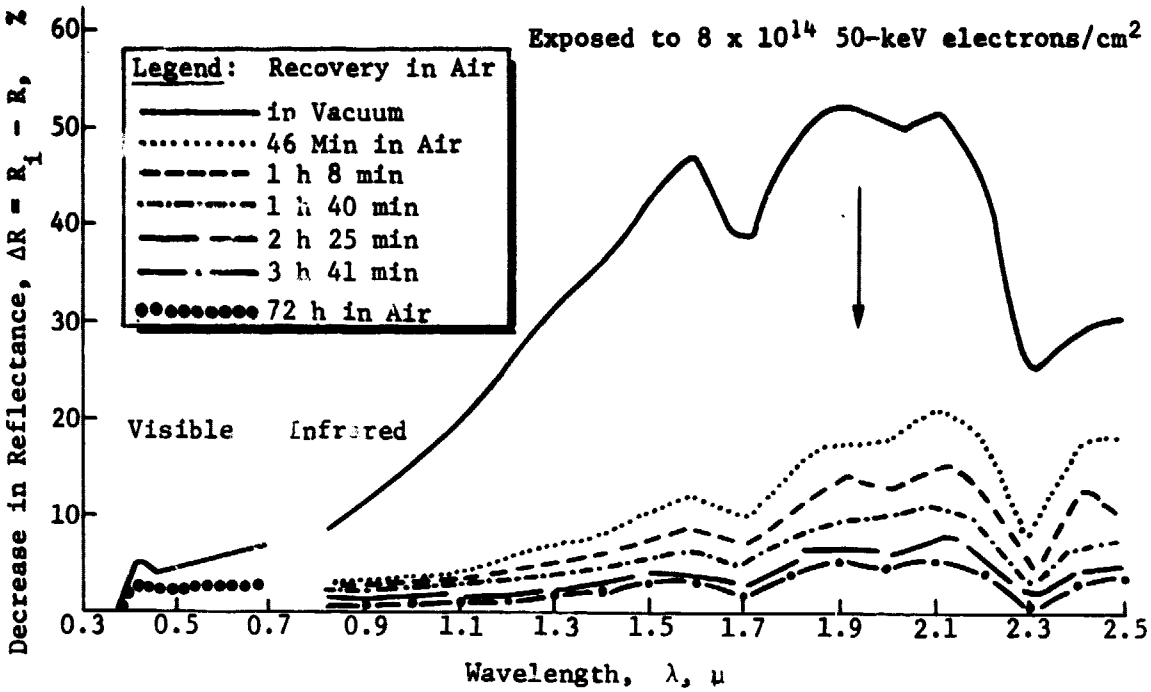

Figure B-4
Damage Profile in S-13G Due to Electron Exposure and Reflectance Recovery in Air

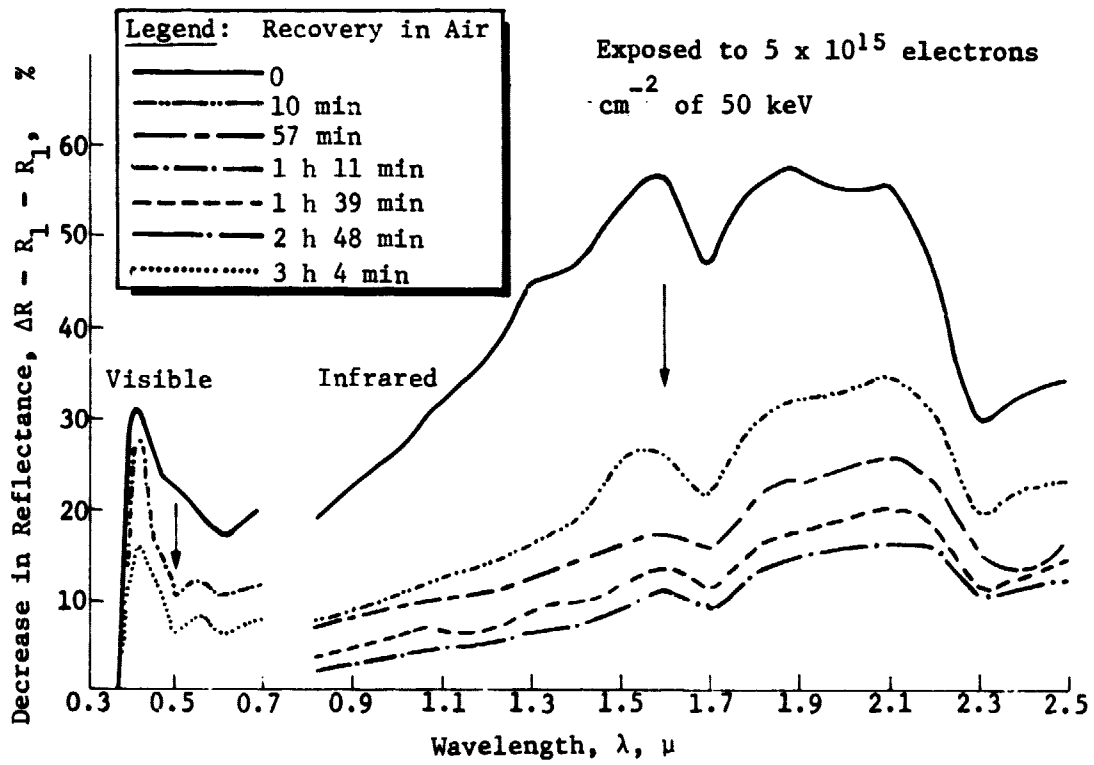

Figure B-5
Postirradiation Reflectance Recovery Properties of S-13G When Reexposed to Air

c. Combined Electron and UV Radiation - Table B-3 shows spectral changes in S-13 after four types of exposure--ultraviolet only, electron only, ultraviolet followed by electron, and simultaneous ultraviolet and electron. All UV exposures were 18 ESH and all electron exposures were 5×10^{14} electrons cm^2. Sequential exposures were done with the samples remaining in situ in the vacuum exposure chamber.

Table B-3 Decrease in Reflectance in S-13 (Ref 10)

Measured After Exposure to	$\Delta R = R_i - R_f$ at Selected Wavelengths, %						
	425 mμ	590 mμ	950 mμ	1200 mμ	1550 mμ	2100 mμ	2300 mμ
UV Only	1	1	3	6	10	22	14
Electrons Only	0	2	6	11	20	37	26
Arithmetic Sum of Above	1	3	9	17	30	59	40
Consecutive Exposure to UV, Then to Electrons	0	2	4	7	15	30	19
Simultaneous UV/Electron Exposure	0	2	7	12	24	43	30

When S-13 is first exposed to electron and then to ultraviolet radiation, it does not recover. However, the 18 ESH of ultraviolet exposure has little additional effect on the reflectance beyond the losses already sustained due to the electron exposure (Fig. B-6). This is reminiscent of the results for the inverse exposure depicted in Table B-3.

The extent of degradation also appears to depend on the ratio of exposure rates of electron and ultraviolet radiation. S-13 was exposed to 18 ESH at a 4.4-ultraviolet-sun rate (total exposure time 4.1 hours). Simultaneously, it received a fluence of 5×10^4 electrons/cm^2 programmed so about 90 percent occurred during the first hour of ultraviolet exposure, and the remaining 10 percent during the final 3.1 hours of ultraviolet exposure. The spectral reflectance was measured after the first hour. Measurements made after the complete exposure of 4.1 hours shows evidence of reflectance recovery (Fig. B-7).

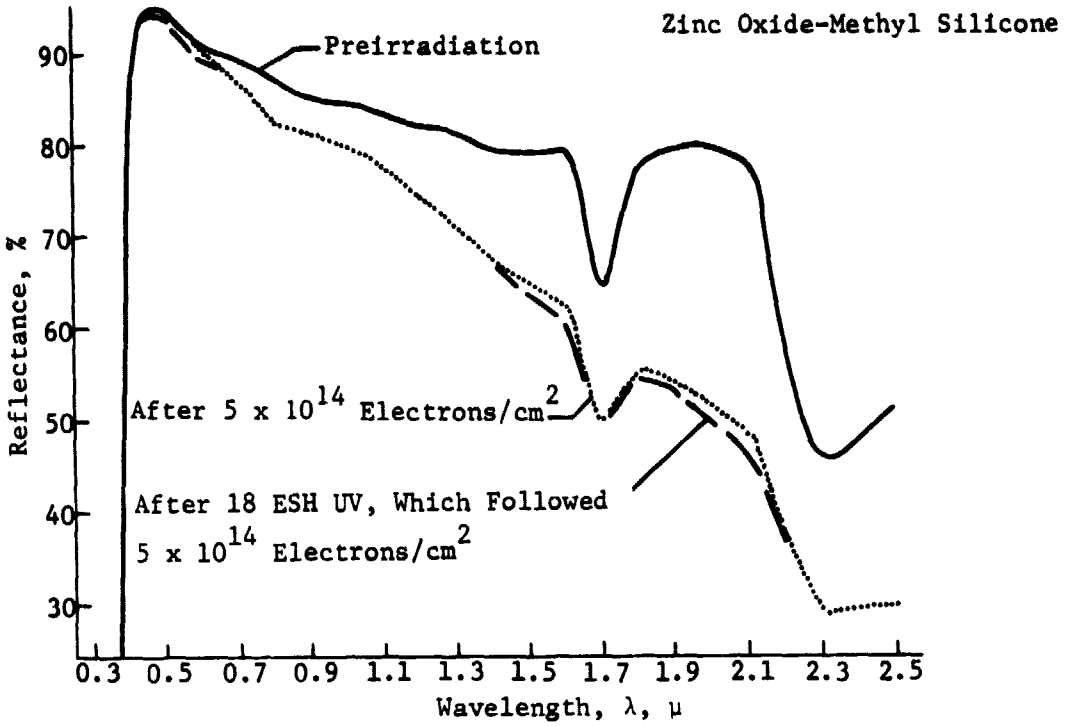

Figure B-6
Spectral Reflectance of S-13 Following Consecutive Exposure to 50-keV Electrons, Then to Ultraviolet Radiation (Ref 10)

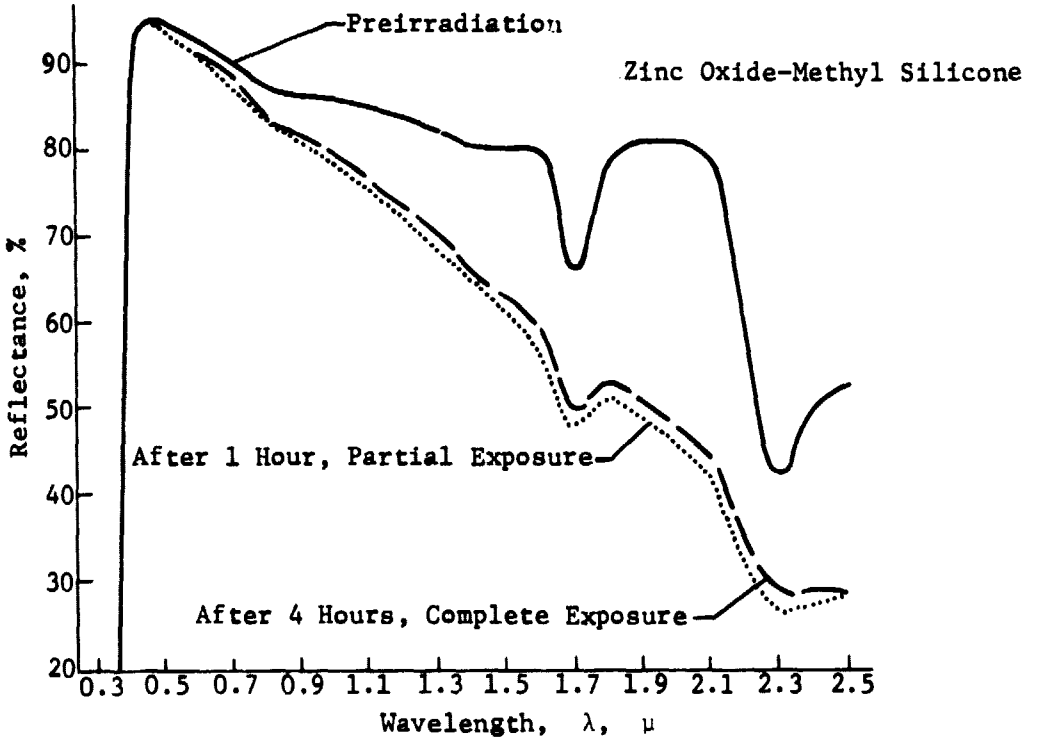

Figure B-7
Spectral Reflectance of S-13 and Effects of Changing the Electron/Ultraviolet Exposure Ratio Midway through Test (Ref 10)

d. Proton and Combined Proton/UV Radiation - Changes in α_s in simulated solar wind proton, simulated solar ultraviolet irradiation, and the combined environment are shown (Ref 12) in Table B-4. In the combined environment at fluxes below 3×10^{16} protons/cm^2 and less than 1000 sun hours there is less total change than in the ultraviolet alone.

Irradiation with 20-keV protons of S-13G showed (Ref 10) that it sustains severe degradation of reflectance in the visible after exposure to 10^{16} protons/cm^2. However the threshold for damage was in the 10^{14} protons/cm^2 range, and even at 10^{15} protons/cm^2 the reflectance degradation was moderate. The buildup of damage and the extent of recovery in air following exposure are shown in Figure B-8. Only partial recovery of reflectance occurs in air.

e. Summary - Wavelength regions in which the largest reflectance changes occur are substantially different for ultraviolet, electron, and proton radiation. Exposure to electrons causes the greatest reflectance losses in the infrared. Ultraviolet radiation and proton radiation result in more damage at shorter wavelengths, particularly at any existing ultraviolet absorption edge.

Table B-4
*Changes in Solar Absorptance of S-13 in Simulated Solar Wind Protons and Ultraviolet Radiations**

Material	Proton Exposure		Ultraviolet Exposure		UV and Proton Exposure	
	Simulated Protons/cm^2 at 2000-eV Energy	Change in Solar Absorptance, %	Ultraviolet Sun-Hours (18-Sun Intensity) +	Change in Solar Absorptance, %	UV Sun-Hours and Protons/cm^2	Change in Solar Absorptance, %
S-13	0.43×10^{15}	5.6	90	44.0	$90/0.28 \times 10^{16}$	33.3
	1.3×10^{15}	11.0	432	56.0	$432/1.1 \times 10^{16}$	50.0
	3.0×10^{16}	56.0	1098	61.0	$1098/2.8 \times 10^{16}$	106.0

* Measurements of absorptance of materials at 0.5 - 1.8 μ in vacuum of 10^{-7} torr.

\+ Intensity corresponds to 18 times the solar ultraviolet (2200 - 4000 A) intensity at distance of earth in space at zero airmass.

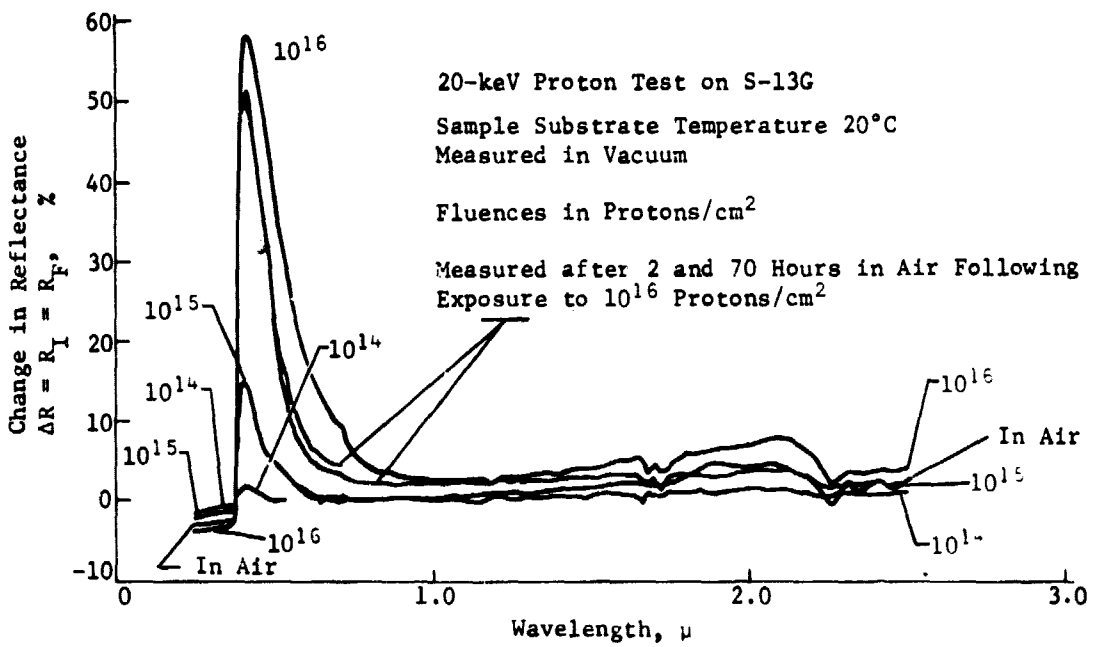

Figure B-8 Buildup of 20-keV Proton Damage in S-13G (Ref 10)

Reflectance recoveries after exposure to air following ultraviolet, electron, and proton exposure are likewise diverse. This diversity of both reflectance and recovery phenomena is indicative of more than one damage mechanism.

The sequencing of combined environment exposures to more nearly simulate space effects significantly alters the resulting degradation. These synergistic effects must be considered in testing for space applications.

B. TEFLON AND KAPTON

This section first presents information concerning "untreated" materials and then data for metalized films.

1. Untreated Teflon and Kapton

a. Thermal-Vacuum Degradation - Thermal degradation under vacuum can be described by simple first-order kinetics. Decomposition begins near 400°C with activation energies (Ref 4) of 70 to 80 kcal for Teflon and about 20 kcal for Kapton. Pertinent pages from Reference 4 are tabulated. These include mass spectral data as a function of temperature.

Material	Pages (Inclusive)
Kapton H Film	Pi1 - Pi5
Teflon Lacing Tape	T1 - T6
Teflon Sheet TFE	T7 - T10
Teflon Tubing FEP	T11 - T14

The TWL range (Ref 2) for Teflon is from 0.00 to 1.53 percent and for Kapton is 0.3 to 1.4 percent. The VCM range (Ref 2) for Teflon is from 0.00 to 0.51 percent and 0.00 to 0.23 percent for Kapton.

b. Optical Changes

Ultraviolet Radiation - Kapton H irradiated with the Boeing UV source previously described shows some reflection losses, but the changes are moderate with some increases and decreases in the visible and infrared regions. Recovery in dry air (Ref 10) is shown in Figure B-9. It can be seen that in the IR the in-air reflectance values are equal to or greater than than the in situ values.

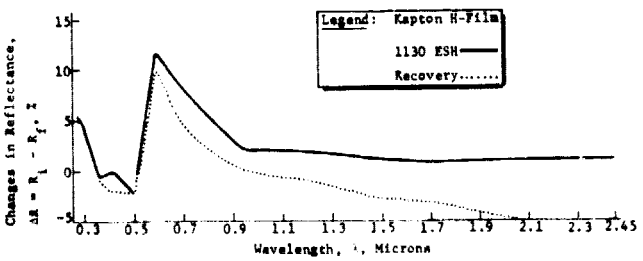

Figure B-9
Reflectance Recovery in Kapton H-Film in Air As a Function of Wavelength, Following Exposure to Ultraviolet Radiation (Ref 10)

However, another investigation (Ref 14) found there was no effect on the transmission of Kapton (1.5 mil) after 9500 ESH with a source of high- and low-pressure mercury arcs, irradiation being under vacuum at 31°C. Transmission tests extended over the range from 350 to 750 nm. Teflon (1.5 mil) suffered only a mild degradation (~10 percent) over the same parameters.

Electron Irradiation - Under electron irradiation Kapton showed (Ref 10) some reflectance losses but serious degradation occurred only at the highest fluences. Table B-5 shows the reflectance changes at 590 nanometers.

Table B-5
Decrease in Reflectance at 590 nm for 50-keV Electrons (Ref 10)

Exposure, electrons/cm^2					
1×10^{13}	1.6×10^{13}	2×10^{14}	5.5×10^{14}	8×10^{14}	8×10^{15}
0	1	4	13	9	60

With 1-MeV electrons Kapton and Teflon were unaffected (Ref 14) up to 2.6×10^{17} electrons/cm^2.

Proton Irradiation - With 800-keV protons Kapton and Teflon were unaffected (Ref 14) up to 10^{14} protons/cm^2.

c. Physical Property Changes

Electron Irradiation, Mechanical Properties - Changes in Teflon induced by irradiation have been assessed by measuring the tensile and flexural characteristics before and after electron irradiation under vacuum (Ref 15). These properties were measured in air. The irradiations were carried out with a Van de Graff accelerator that produced a continous beam of electrons.

Samples were irradiated to doses up to 10 Mrad at a rate of 395 rad/s, and measurements of mechanical properties were made after approximately 24 hours in air. Figure B-10 shows that the tensile and flexural modulus increase with dose to approximately the same ext

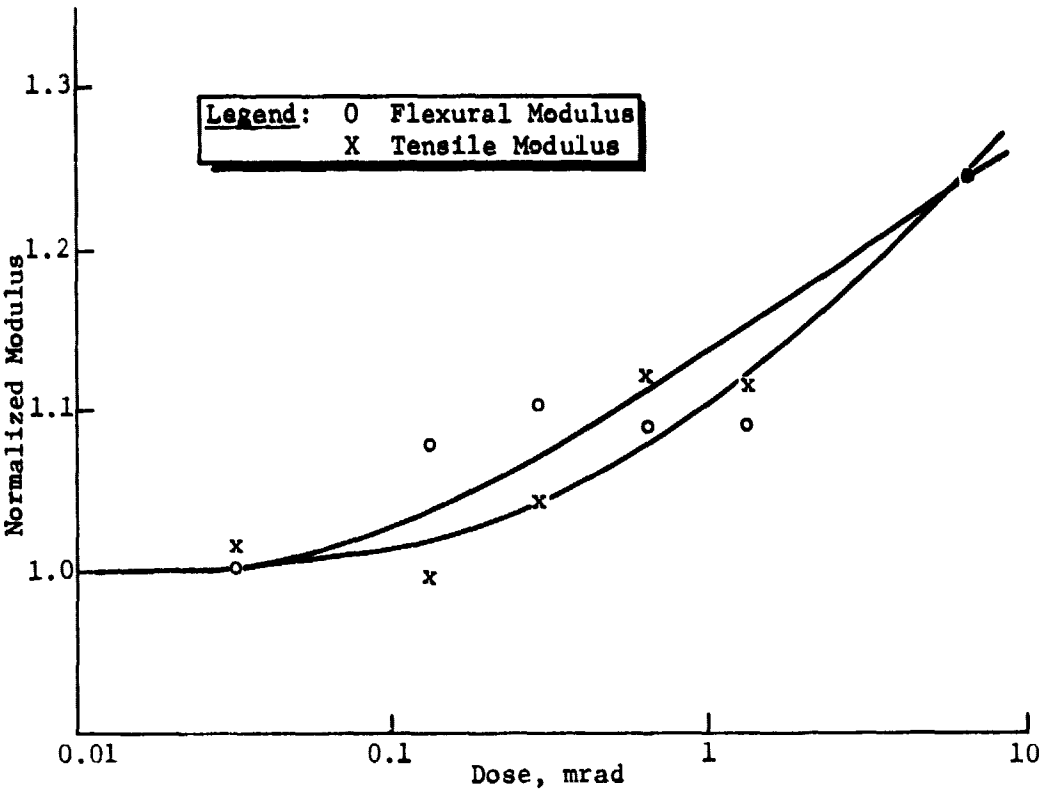

Figure B-10
Flexural and Tensile Moduli As a Function of Dose (Ref 15)

Figure B-11 shows the changes in tensile strength and extension. Samples irradiated to a dose of 1 Mrad with 1-MeV electrons at dose rates ranging from 84 to 7462 rad/s showed that the dose rate has no effect on the resulting change in mechanical properties. Varying the electron energy between 0.4 and 1.8 MeV showed the mechanical properties are also independent of the electron energy. For comparison, data on strength and dose from an unclassified portion of a classified report (Ref 16) are also included in Figure B-11. It can be seen that the low-energy irradiations appear to behave in a similar manner.

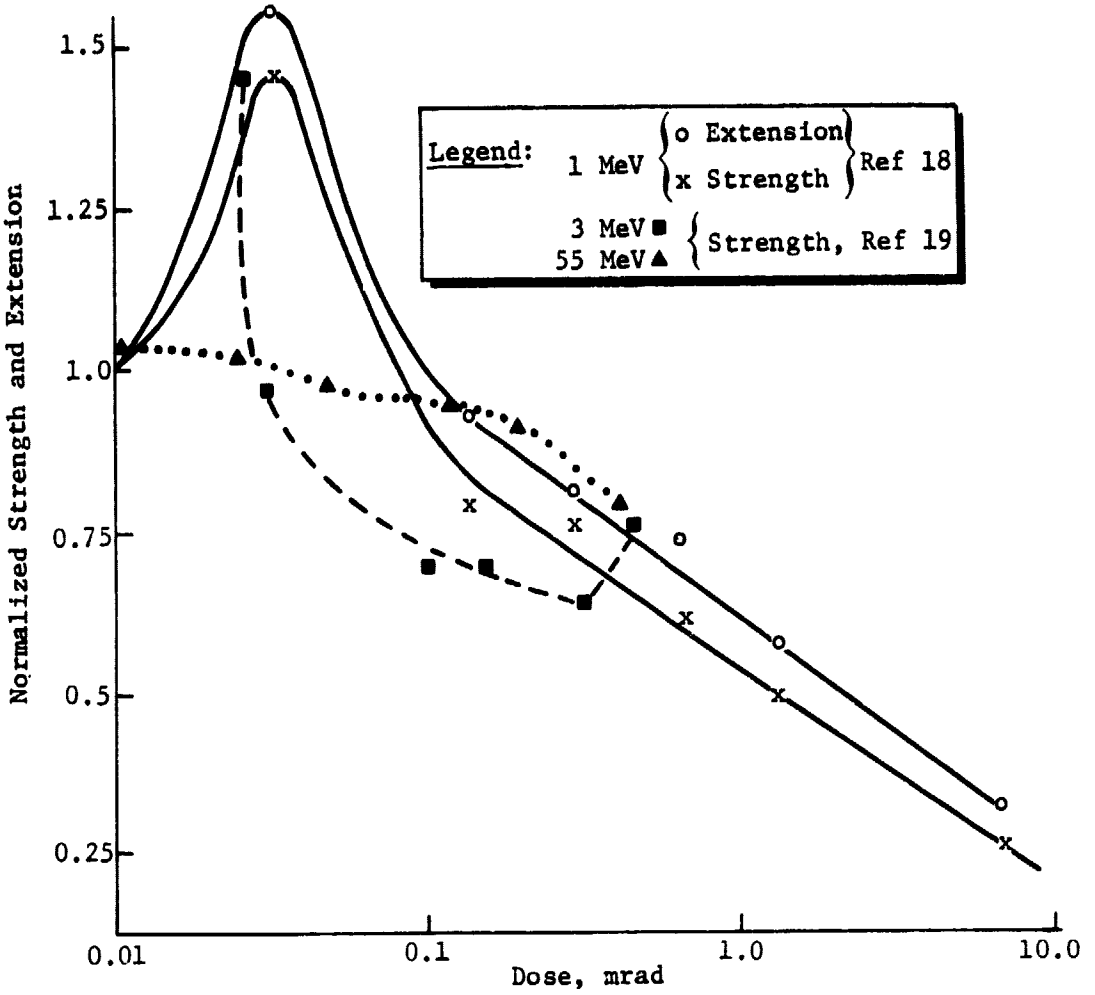

Figure B-11
Tensile Strength and Extension to Failure (Ref 15) and Tensile Strength at 50% Elongation As a Function of Dose (Ref 16)

Electron Irradiation, Electrical Properties - Changes in electrical properties of Teflon after electron irradiation have been obtained from unclassified portions of Reference 16. Although the irradiations were done at 22°C and 760 torr, the results are included here for completeness. Table B-6 shows the changes in electrical conductivity as a function of dose with 3- and 55-MeV electrons, and Table B-7 shows the changes in the dielectric constant.

Table B-6
*Pre/Postirradiation Conductivity at Electric Field of 20 V/mil**

Electron Energy, MeV	Material	Nominal Dose, rads - Teflon					
		2×10^4		1×10^5		5×10^5	
		Pre	Post	Pre	Post	Pre	Post
3	1	<1.4	1.7	<1.7	1.8	1.7	1.9
	2	1.6	1.5	1.5	1.8	1.6	2.1
	3	<1.3	<1.3	<1.4	1.5	<1.6	4.2
55	1	<1.3	2.4	<1.3	1.9	<1.3	2.4
	2	<1.3	2.0	<1.3	1.8	<1.3	2.1
	3	<1.8	2.4	2.8	4.2	<1.3	2.2

* Materials: 1 - TFE-7; 2 - TFE-6C; 3 - FEP-100.
Units of conductivity, 10^{-17} $(\text{ohm-cm})^{-1}$.
All values average of three samples.

Table B-7
Percentage Change in Dielectric Constant As a Function of Frequency and Absorbed Dose (22°C, 760 torr)

Electron Energy, MeV	Frequency, Hz	Material*	Nominal Dose, rads - Teflon		
			2×10^4	1×10^5	5×10^5
3	10^2	1	-4.11	-3.31	-4.39
		2	-4.21	-3.02	-3.10
		3	-2.50	-0.98	+1.02
	10^3	1	-4.06	-3.31	-3.10
		2	-4.19	-3.02	-3.10
		3	-2.55	-0.98	+1.01
	10^4	1	-4.03	-3.28	-2.97
		2	-4.19	-3.01	-3.08
		3	-2.56	-0.99	+1.00
	10^5	1	-4.03	-3.27	-3.03
		2	-4.17	-2.98	-3.06
		3	-2.57	-1.02	+0.98
55	10^2	1	+0.25	+0.69	+1.27
		2	-2.30	-2.84	-3.85
		3	-2.80	-1.52	+0.22
	10^3	1	+0.03	-0.57	+0.39
		2	-0.79	-2.85	-3.59
		3	-3.06	-1.68	-0.06
	10^4	1	-0.27	+0.47	+0.49
		2	-2.45	-3.42	-3.84
		3	-3.04	-1.75	-0.65
	10^5	1	-0.34	+0.55	+0.46
		2	-2.33	-3.45	-3.84
		3	-3.15	-1.57	-0.56

* Material: 1 - TFE-7; 2 - TFE-6C; 3 - FEP-100.

Simultaneous UV and Particle Irradiation, Optical Properties - Figure B-12 shows (Ref 17) the effects of simultaneous irradiation on the solar absorbtance of 5-mil FEP Teflon. Simulations A, B, and C are for earth-orbit conditions, and simulation D is for solar wind.

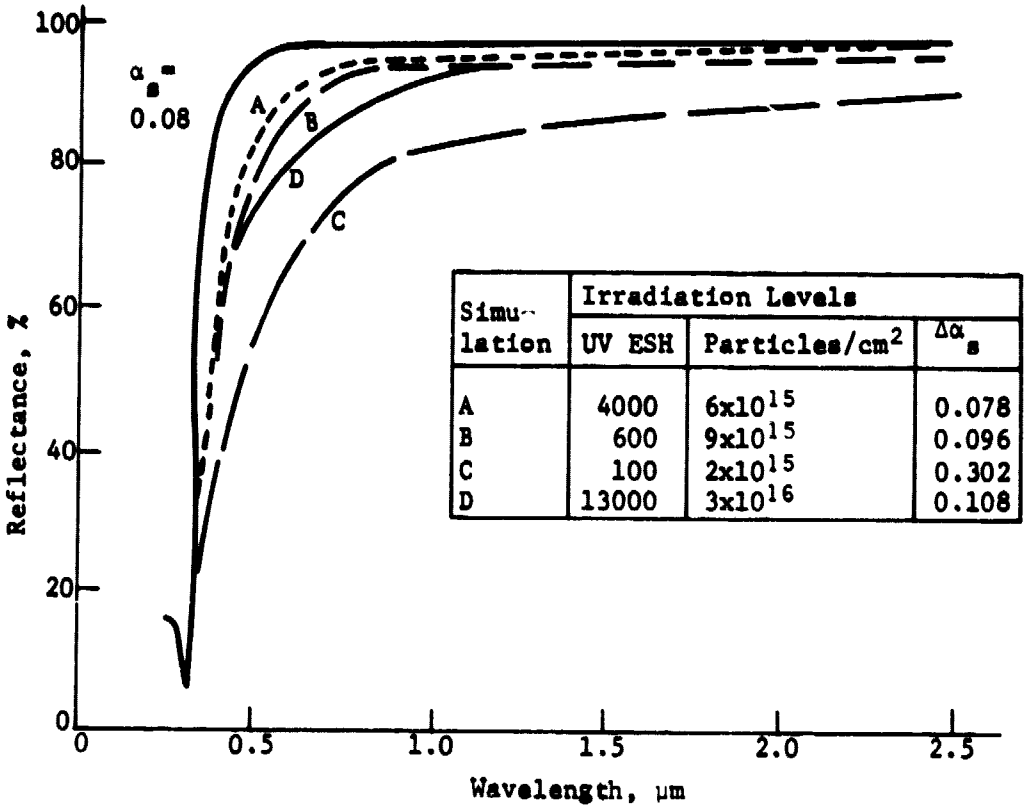

Simulation	Irradiation Levels		
	UV ESH	Particles/cm^2	$\Delta\alpha_s$
A	4000	6×10^{15}	0.078
B	600	9×10^{15}	0.096
C	100	2×10^{15}	0.302
D	13000	3×10^{16}	0.108

Figure B-12
Effects of UV, Electrons, and Protons on 5-mil FEP Teflon (Ref 17)

Simulation A is at a UV irradiation rate of one-sun plus charged particles (electrons and protons) at rates of 2×10^8 (e + p) cm^{-2} s^{-1}. Simulation B considers a smaller fraction of a year orbital time with magnetic substorm conditions, i.e., one-sun UV plus electrons and protons at a rate of 2×10^9 (e + p) cm^{-2} s^{-1}. Simulation C has fluxes increased to peak orbital values of 3×10^9 electrons cm^{-2} s^{-1} and the same flux for protons. The originally transparent film becomes translucent or even opaque with irradiation. A simulated solar wind is given as Simulation D with a flux of 1×10^{10} protons cm^{-2} s^{-1} combined with UV radiation. With this intensity of irradiation, the Teflon's visual appearance becomes that of a white paint.

A sample of FEP Teflon was flown on Skylab D024. Transmission losses in the UV-visible were attributed (Ref 11) to contamination.

Simultaneous UV and Particle Irradiation, Mechanical Properties - Irradiation with 1-MeV electrons and simulated solar radiation (2.66 kW m^{-2} xenon lamp) indicated (Ref 15) that the predominant effect of the UV radiation on mechanical properties will be the influence of the rise in temperature of the sample on the effects of the electron irradiation.

Teflon TFE and FEP samples from Surveyor III were returned (Ref 18) from the moon by Apollo XII. Teflon FEP appeared to suffer only a small degradation in tensile strength whereas TFE cable wrap was appreciably degraded with tensile strength decreased by 75 percent and elongation by 60 percent.

Results derived (Ref 19) from the Skylab D024 experiment are depicted in Figure B-13. It is of interest to compare this figure with the tensile strength data presented in Figure B-11.

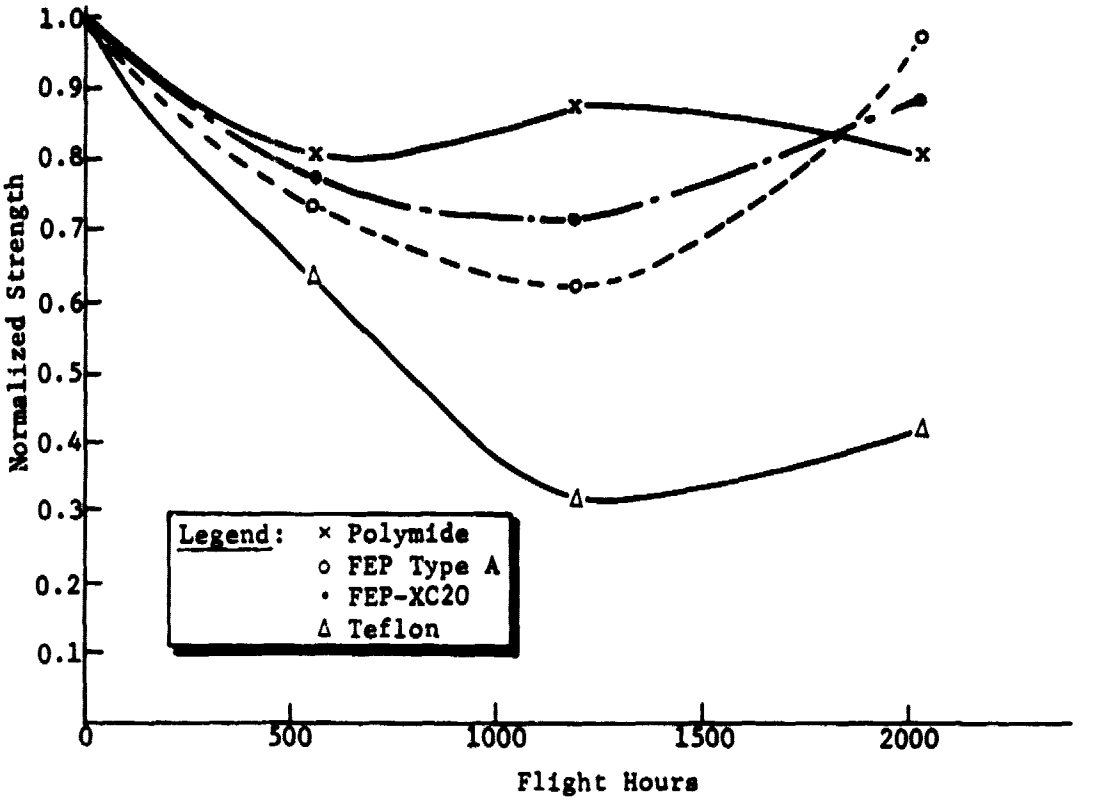

Figure B-13
Tensile Strength As a Function of Time during Skylab D024 Experiment

2. Metalized Teflon and Kapton Films

The survey of these materials under solar simulation is dominated by the extensive studies of Boeing (Ref 20) and TRW (Ref 21). The Boeing group studied optical properties up to 910 ESH, and the TRW group extended the times to years. The TRW group also studied mechanical properties under the same simulation.

a. Optical Properties - Most irradiation data have been obtained for 5-mil thicknesses of Teflon film. There is evidence that thinner films may have more resistance to dielectric breakdown. If they are thin enough not to trap energetic charged particles, they have more favorable reflectance properties. Figure B-14, derived from the Boeing studies, (Ref 17), compares 5-mil and 2-mil metalized films and shows such an effect.

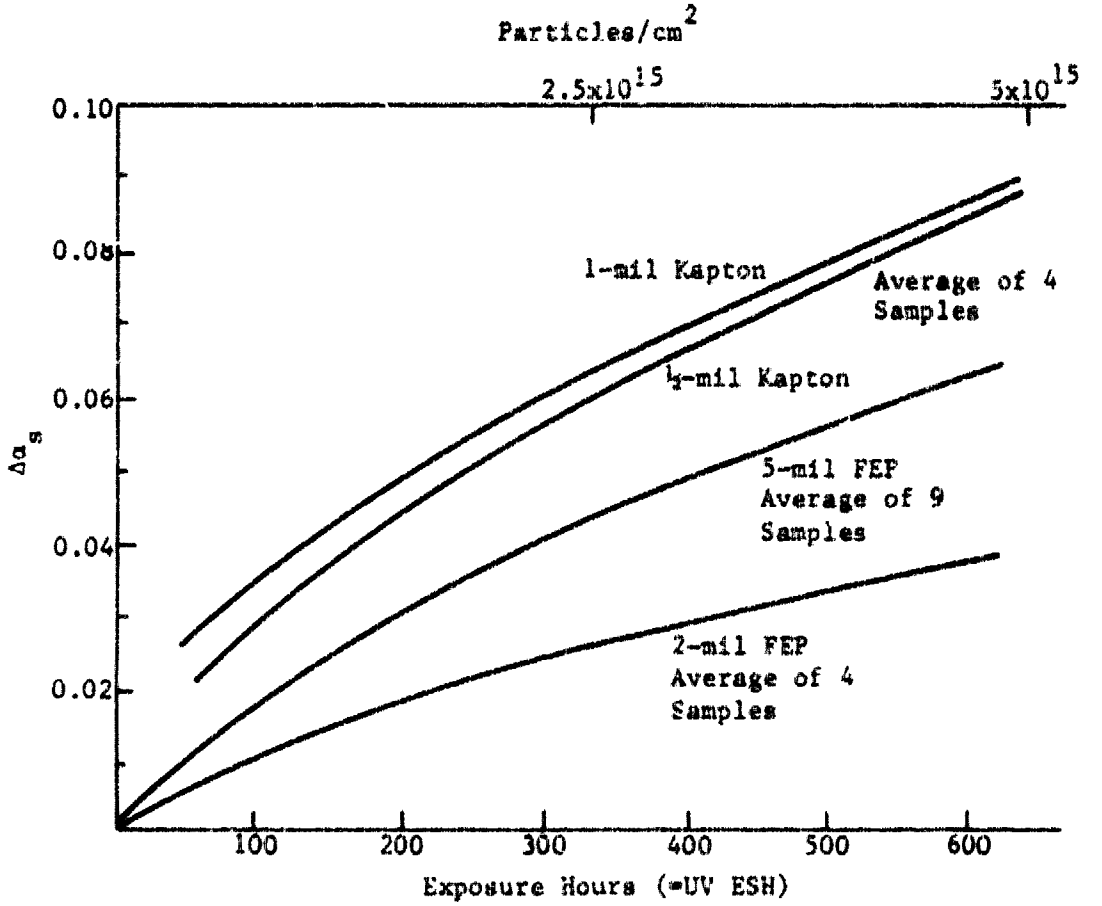

Figure B-14
Reflectance Stability of Kapton and FEP Teflon Exposed to UV, 115-keV Electrons, and 50-keV Protons (Equal Fluences of Each Type of Particle)

Such effects do not occur (Ref 20) when metalized films are irradiated by lower energy charged particles simultaneously with UV. Figure B-15 shows that 2-mil and 5-mil film appear to be more nearly alike under these conditions. Figure B-14 also shows the results of 1/2-mil and 1-mil Kapton, that may be compared with the Teflon film data.

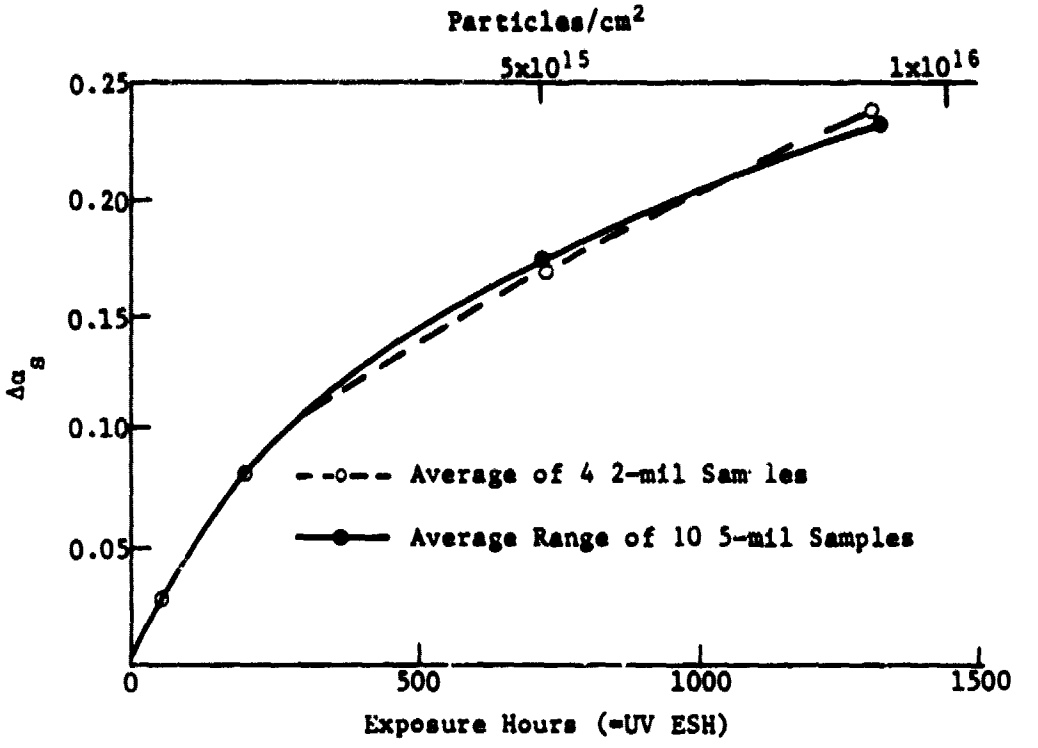

Figure B-16
Solar Absorptance of Metalized 2-mil and 5-mil FEP Films Irradiated by 30-keV Electrons, 20-keV Protons, and UV Equal Fluences of Each Particle (Ref 20)

Similar metalized films were studied for longer times by the TRW group (Ref 21). Figure B-16 was derived from their data. As with the shorter time exposures, the changes in solar absorptance increase with time. Normal emittances, measured in air, after three years of equivalent space exposure remain virtually unchanged.

b. Mechanical Properties - Extensive testing of metalized Teflon and Kapton films was done by the TRW group (Ref 21) under near-UV, 80 and 200-keV electrons simultaneously under vacuum. Mechanical properties were tested both in situ and ex situ.

Results indicated that FEP and PFA Teflon materials exhibited brittle behavior after 18 months of equivalent exposure. By a 30-month equivalent exposure, essentially all Teflon materials had experienced a complete loss of elongation. The Kapton materials experienced a 25 to 40 percent reduction in ultimate elongation but had only small changes in modulus and ultimate strength. No brittle failure occurred during the entire test program. The in situ and ex situ tensile test results were qualitatively consistent (i.e., Teflon exhibited catastrophic degradation in mechanical properties while Kapton exhibited only some degradation), although the rate of degradation for Teflon in the in situ chamber was less than that for the ex situ specimens. This difference suggests that return of irradiated specimens to atmospheric conditions before testing may affect the measured properties.

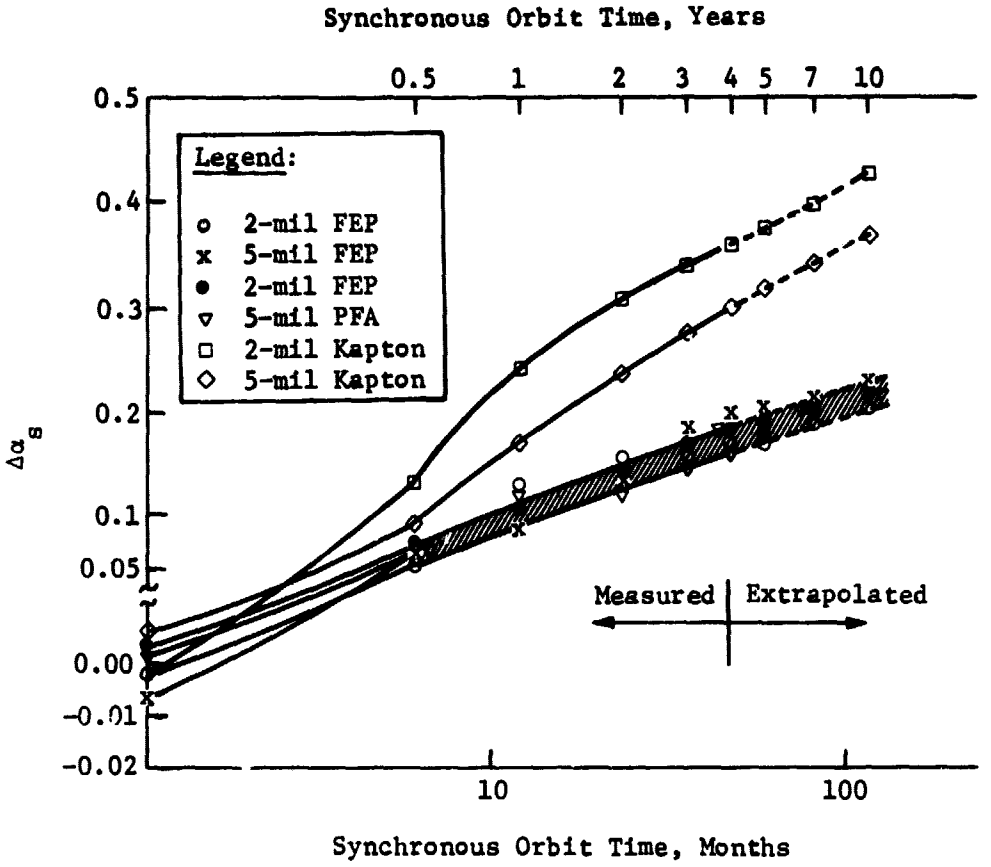

Figure B-16
Changes in Solar Absorptance Characteristics of Metalized Films of Teflon and Kapton As a Function of Time (Radiation Near-UV and Far-UV, 27-keV Protons, 7, 80, and 200-keV Electrons; Points Are Average of 3 Samples Each)

Tensile properties were sensitive to specimen size. Table B-8 summarizes the key results.

Radiation exposures were carried out with 1-inch gage lengths. Table B-9 shows the in situ secant modulus changes under simultaneous UV and 80 and 200-keV electrons.

These results may be compared with the ex situ results presented in Table B-10.

Table B-8

*Effect of Tensile Specimen Gage Length on Tensile Properties**

	1-in. Gage Length			4-in. Gage Length			Ratios†		
Material	Modulus, ksi	Ultimate Strength, ksi	Ultimate Elongation, %	Modulus, ksi	Ultimate Strength, ksi	Ultimate Elongation, %	E_4/E_1	σ_4/σ_1	$\varepsilon_4/\varepsilon_1$
20FEPAGIN	66.9	3.1	480.0	89.6	2.1	216.5	1.34	0.68	0.45
50FEPAGIN	57.4	3.5	422.0	75.8	2.8	343.0	1.32	0.80	0.55
20KAL	342.5	23.9	66.5	501.0	20.4	18.0	1.46	0.85	0.27
50KAL	324.0	24.9	75.0	485.0	21.3	25.5	1.50	0.85	0.34

* Average machine and transverse direction properties, three specimens per each direction.

† E = modulus, σ ultimate strength, ε = elongation, subscripts 1 and 4 represent values for 1- and 4-inch gage lengths, respectively.

Table B-9

*In situ Secant Modulus (E_2) at 2% Strain, ksi**,†*

	Exposure, Months					
Materials	0	6	12	18	24	30
2-mil FEP	87	85	88	100	103(1.7%)¶	
5-mil FEP	77	78	78	84	84	71(1.6%)¶
5-mil PFA	64	67	66	72	82	85(1.4%)¶
2-mil Kapton	343	355	349	352	360	335
5-mil Kapton	341	341	353	298	345	313

* E_2 = Stress at 2% Strain/0.02 in ksi.

† Most Results Average of 2 to 3 Specimens.

¶ (XX) indicates that sample failed at XX% strain.

Specimen Identification

2-mil FEP Teflon with Vacuum-Deposited Silver and Inconel

5-mil FEP Teflon with Vacuum-Deposited Silver and Inconel

5-mil PFA Teflon with Vacuum-Deposited Silver and Inconel

2-mil Kapton with Vacuum-Deposited Aluminum

5-mil Kapton with Vacuum-Deposited Aluminum

Table B-10 Ex situ Secant Modulus (E_2) at 2% Strain, ksi†*

	Exposure, Months					
Materials	0	6	12	17	30	36
2-mil FEP	71	92	73	§	§	§
5-mil FEP	57	72	62	59	§	§
5-mil PFA	51	72		§	§	
2-mil Kapton	324	353	315		360	
5-mil Kapton	345	360	293		285	

* Tensile tested to failure in air; air exposure duration between 1 and 20 minutes.

† Average of 3 specimens in machine direction.

§ Irradiated specimen brittle to the touch; no tensile test possible.

Tensile properties under these exposures are presented in Tables B-11 and B-12.

*Table B-11 In situ Tensile Properties at Failure**

	Elongation, %			Tensile Strength, psi		
	Exposure, Months					
Materials	0	9	39	0	9	39
2-mil FEP	473	45		3470	2500	
5-mil FEP	650	105†		3660	2200†	
5-mil PFA	659	55	109	4725	2440	2240
2-mil Kapton	68		35	24750		23350
5-mil Kapton	91		60	2720		26800

* Most results average of 2 specimens.

† No failure; stress and elongation at maximum head travel of testing equipment.

Table B-12 *Ex situ Tensile Properties at Failure*[*,†]

	Exposure, Months											
	Elongation, %						Tensile Strength, psi					
Material	0	6	12	17	30	36	0	6	12	17	30	36
2-mil FEP	473	6	2.7	1.5	§	§	3470	2150	1985¶	§	§	§
5-mil FEP	648	7	18	4.8	§	§	3660	1900	1890	1690	§	§
5-mil PFA	661	9	134	¶	§		4420	2000	2060	§	§	
2-mil Kapton	68	60	73				24750	26800	27000		26500	
5-mil Kapton	91	80	80				27200	30400	28300		26400	

* Most results average of 2 specimens.
† Tensile tested to failure in air; air exposure duration between 1 and 20 minutes.
§ Irradiated specimen brittle to the touch; no tensile test possible.
¶ Samples failed at 4% strain.

3. Conclusions

Some conclusions that may be drawn from these results are as follows. The use of Teflon materials for thermal control purposes or in applications requiring flexibility after exposure is not recommended for space. Kapton materials experienced a doubling in α_s, became black, and exhibited a 25 to 40 percent reduction in ultimate elongation, a slight reduction in tensile strength, and a negligible change in modulus. These changes, however, are not deemed catastrophic enough to eliminate its continued use in space systems.

Changes in optical and thermophysical properties for Teflon and Kapton are primarily due to low-energy proton radiation and/or its synergistic combination with other environmental components.

The discoloration of Teflon and Kapton is limited to the upper layer of exposed material. Light scratching of the surface removes the discoloration, revealing clear material underneath. This result supports the contention that protons are the primary cause of the optical degradation [proton penetration depth is less than 0.3 μm ($\sim$0.01 mil)]

Catastrophic changes in mechanical properties for Teflon are primarily due to near-ultraviolet radiation and/or its synergistic combination with high-energy electrons. Specimens exposed to five-year equivalent electron radiation retain a percentage of their original ultimate elongation, while all specimens subjected to combined near-ultraviolet and high-energy electron radiation become brittle after 17 to 30 months of exposure.

Changes in mechanical properties for Kapton are primarily due to near-ultraviolet radiation and/or its synergistic combination with high-energy electrons. Specimens exposed to five-year equivalent electron radiation show a negligible change in mechanical properties; however, combined near-ultraviolet and high-energy electron radiations result in a measurable, but not catastrophic, reduction in ultimate elongation.

REFERENCES

1. J. A. Thorne and C. L. Whipple: "Silicones in Outer Space." Paper presented at SAMPE 11th National Symposium, St Louis, MO, 1967.

2. Compilation of VCM Data of Nonmetallic Materials. NASA-JSC-08962, 1978.

3. H. A. Papazian: "Predictions of Polymer Degradation Kinetics at Moderate Temperatures from TGA Measurements." J. Appl. Polym. Sci., 16, 2503, 1972.

4. Nonmetallic Materials Handbook. NAS1-13177, 1974.

5. H. A. Papazain: Predictive Testing of Nonmetallic Materials, SERI Contract XH-9-8191-1, 1980.

6. D. J. Progar and W. R. Wade: Vacuum and Ultraviolet Radiation Effects on Binders and Pigments for Spacecraft Thermal Control Coatings. NASATND6546, 1971.

7. J. P. Millard and B. D. Pearson Jr.: "Optical Stability of Coatings Exposed to a Four-Year Space Environment on OSO-III." Paper presented at AIAA 8th Thermophysics Conference, Palm Springs, CA, 1973.

8. W. G. Kirby and D. W. Mills, Jr.: The Effects of Proton Irradiation Rate on the Solar Transmittance of a Thermal Control Binder Material. AEDC-TR-70-257, 1970.

9. D. B. Pearson, Jr.: "Preliminary Results from the Ames Emissivity Experiment on OSO-II." Progress in Astronautics and Aeronautics, Vol 18, Academic Press, New York, NY, 1966.

10. L. B. Fogdall and S. S. Cannaday: In Situ Electron, Proton, and Ultraviolet Effects on Thermal Control Coatings. Contract NAS5-9650, 1968.

11. W. L. Lehn and C. J. Hurley: "Skylab D024 Thermal Control Coatings and Polymeric Films Experiment." Paper presented at AIAA/AGU Conference on Scientific Experiments of Skylab, Huntsville, AL, 1974.

12. Space Materials Handbook. NASA SP-3051, 1969.

13. J. A. Bass: Ultraviolet Radiation Effects on the Infrared Damage Rate of a Thermal Control Coating. NASA TM-X-65704, 1971.

14. E. Anagnostou and A. E. Spakowski: "The Effect of Electrons, Protons, and Ultraviolet Radiation on Plastic Materials." Paper presented at Eighth IEEE Photovoltaic Specialists Conference, Seattle, WA, 1970.

15. D. Verdin and P. R. Goggin: The Effects of Radiation on the Mechanical and Electrical Properties of the GEOS Satellite Long-Boom Cable Materials. ESTEC Contract No.2082/73 SK, 1975. (N76-13298)

16. E. A. Szymkowiak, D. R. Sukis, and S. E. Harrison: Transient Radiation Effects of Selected Properties of Teflon. ECOM Technical Report -0450-F. (Classified)

17. L. B. Fogdall, S. S. Cannaday, and W. S. Slemp: "Effects of Space Radiation on Thin Polymers and Nonmetallics." Paper presented at AIAA 12th Thermophysics Conference, Albuquerque, NM, 1977.

18. Surveyor III Returned from the Moon by Apollo XII. Hughes Aircraft Company, 1970.

19. C. J. Hurley and W. L. Lehn: "Results of the Polymeric Films Skylab D024 Experiment." Paper presented at AIAA 10th Thermophysics Conference, Denver, CO, 1975.

20. L. B. Fogdall and S. S. Cannaday: Effects of High-Energy Simulated Space Environment on Polymeric Second-Surface Mirrors. Contract NAS1-13530, 1975.

21. R. M. Kurland et al.: Properties of Metalized Flexible Materials in the Space Environment. SAMSO TR78-31, 1978.